Chapter 6 in the book:
P.A. Kralchevsky and K. Nagayama, "Particles at Fluid Interfaces and Membranes"
(Attachment of Colloid Particles and Proteins to Interfaces and Formation of Two-Dimensional Arrays)
Elsevier, Amsterdam, 2001; pp. 248-286.

# CHAPTER 6

## PARTICLES AT INTERFACES:
## DEFORMATIONS AND HYDRODYNAMIC INTERACTIONS

Here we consider some aspects of the interaction of colloidal particles with a phase boundary, which involve deformations of a fluid interface and/or hydrodynamic flows. First, we discuss the energy changes accompanying the collision of a fluid particle (emulsion drop of gas bubble) with an interface or another particle. If the interaction is governed by the surface dilatation and the DLVO forces, the energy of the system may exhibit a minimum, which corresponds to the formation of a floc of two attached fluid particles. If oscillatory-structural forces are operative, then the energy surface exhibits a series of minima separated by barriers, whose physical importance is discussed. The radius of the liquid film formed between a fluid particle and an interface can be determined by means of force balance considerations. For small contact angles the film radius is proportional to the squared radius of the particle.

Next we consider the hydrodynamic interactions of a colloidal particle with an interface (or another particle), which are due to flows in the viscous liquid medium. The theory relates the velocity of mutual approach of the two surfaces with the driving force. The respective relationships depend on the shape of the particle, its deformability and surface mobility. The gradual approach of two fluid particles may terminate when the thickness of the gap between them reaches a certain critical value, at which fluctuation capillary waves spontaneously grow and cause rupturing of the liquid film; the comparison of theory and experiment is discussed.

Finally, we consider the factors and mechanisms for detachment of an oil drop from a solid surface in relation to the process of washing. The destabilization of the oil–water interface and of the three-phase contact line are known as, respectively, "emulsification" and "rolling-up" mechanisms of drop removal. Some surfactants are able to produce penetration of aqueous films between oil and solid, which is a purely physicochemical "disjoining film" mechanism for drop detachment. Attention is paid to the detachment of oil drops from the orifice of a pore in relation to the methods of emulsification by ceramic and glass membranes.

## 6.1. DEFORMATION OF FLUID PARTICLES APPROACHING AN INTERFACE

### 6.1.1. *THERMODYNAMIC ASPECTS OF PARTICLE DEFORMATION*

As demonstrated in Section 5.2.10, the deformation of a droplet at fixed volume leads to an expansion of its surface area, Eq. (5.133). In addition, the flattening of the droplet surfaces in the zone of their contact is accompanied with a variation of the interfacial bending energy of the droplets, Eq. (5.134). Last but not least, the formation of a thin liquid film between the two drops much enhances the role of the surface forces, such as the van der Waals attraction, electrostatic repulsion, oscillatory structural forces, steric interactions, etc., see Section 5.2.

In Ref. [1] it was demonstrated that the energy of interaction between two fluid particles (drops or bubbles) calculated for the model shape of truncated spheres (Fig. 5.19) quantitatively agrees very well with the energy calculated by means of the "real profile", i.e. by accounting for the transition zone between the flat film and the spherical portions of the drop surfaces. Therefore, below we will use the configuration of truncated spheres.

Equation (5.50) with $h_0 \equiv h$ reads:

$$U(h, r_c) = (2\boldsymbol{p}R / j) \int_h^\infty f(\hat{h})\, d\hat{h} + \boldsymbol{p} r_c^2 f(h) \tag{6.1}$$

where $j = 1,2$ for the systems depicted in Fig. 5.19a and 5.19b, respectively. One sees that the energy of interaction between two deformed fluid particles, $U$, depends on two geometrical parameters, the film thickness, $h$, and the film radius, $r_c$. However, it is natural to present the interaction energy as a function of a single parameter, which can be the distance $z$ between the droplets' mass centers, i.e. $U = U(z)$. In the rigorous approach to this problem, the dependence of the interaction energy on the distance $z$ is characterized by the potential of the mean force, $u_{mf}(z) = -kT \ln g(z)$, where, as usual, $k$ is the Boltzmann constant, $T$ is temperature, and $g(z)$ is the pair (radial) correlation function, see Ref. [2]. The latter function is determined by statistical averaging over all possible droplet configurations (of various $h$ and $r_c$) corresponding to a given $z$:

$$g(z) = 1.103 \left( \frac{\boldsymbol{p} R^2 \boldsymbol{s}}{2kT} \right)^{1/4} \frac{1}{R} \int \exp\left\{ -U[h(r_c,z),r_c]/kT \right\} dr_c \tag{6.2}$$

Here $R$ and $\boldsymbol{s}$ are the radius and the interfacial tension of the fluid particle; $h(r_c,z)$ represents the geometrical relation between $h$ and $r_c$ for a given $z$ and fixed drop volume. To calculate $u_{mf}(z)$ one needs to know the function $U = U(h,r_c)$, which may contain contributions due to the various effects mentioned in the beginning of this section.

As an illustration, let us consider the function $U(h,r_c)$ in a typical case, in which the interaction energy between two *identical* emulsion drops (Fig. 5.19b) is determined by the van der Waals attraction, the electrostatic repulsion and the interfacial dilatation:

$$U(h,r_c) \equiv U_{vw} + U_{el} + U_{dil} \tag{6.3}$$

Here $U_{vw}$ and $U_{dil}$ are determined by Eqs. (5.64) and (5.133). To obtain an expression for $U_{el}$ one can substitute $\Pi_{el}(h)$ from Eq. (5.93) into Eq. (5.9), and then the calculated $f_{el}$ − into Eq. (6.1) with $j = 2$; the result reads [1-3]

$$U_{el}(h,r_c) = \frac{64 \boldsymbol{p} n_0 kT}{\boldsymbol{k}} \tanh^2 \left( \frac{Ze \boldsymbol{y}_s}{4kT} \right) \exp(-\boldsymbol{k}h) \left[ r_c^2 + \frac{R}{\boldsymbol{k}} \right]; \qquad \boldsymbol{k}^2 = \frac{8 \boldsymbol{p} Z^2 e^2 n_0}{\boldsymbol{e} kT} \tag{6.4}$$

where $\boldsymbol{k}^{-1}$ is the Debye screening length, $n_0$ is the concentration of a symmetric Z:Z electrolyte, $\boldsymbol{e}$ denotes the dielectric permittivity; $\boldsymbol{y}_s$ is the surface potential of the particle.

Figure 6.1 shows a contour plot of $U(h,r_c)$, calculated by means of Eq. (6.3) with parameter values $R = 1$ μm, $\boldsymbol{y}_s = 100$ mV, $\boldsymbol{s} = 1$ mN/m, $n_0 = 0.1$ M and Hamaker constant $A_H = 2 \times 10^{-20}$ J; the term with the Gibbs elasticity $E_G$ in Eq. (5.133) is neglected. The minimum of the potential surface $U(h,r_c)$ corresponds to an *equilibrium* doublet of two attached drops with a film formed between them; the thickness and the radius of this film will be denoted by $h_{eq}$ and $r_{c,eq}$. The depth of the minimum in Fig. 6.1a is $U(h_{eq}, r_{c,eq}) = -60\, kT$. Hence, the equilibrium doublet should be rather stable. The numerical computations [2] show that the radius of the equilibrium film $r_{c,eq}$, and the area of attachment, increases with the rise of both electrolyte concentration $n_0$ and drop radius $R$.
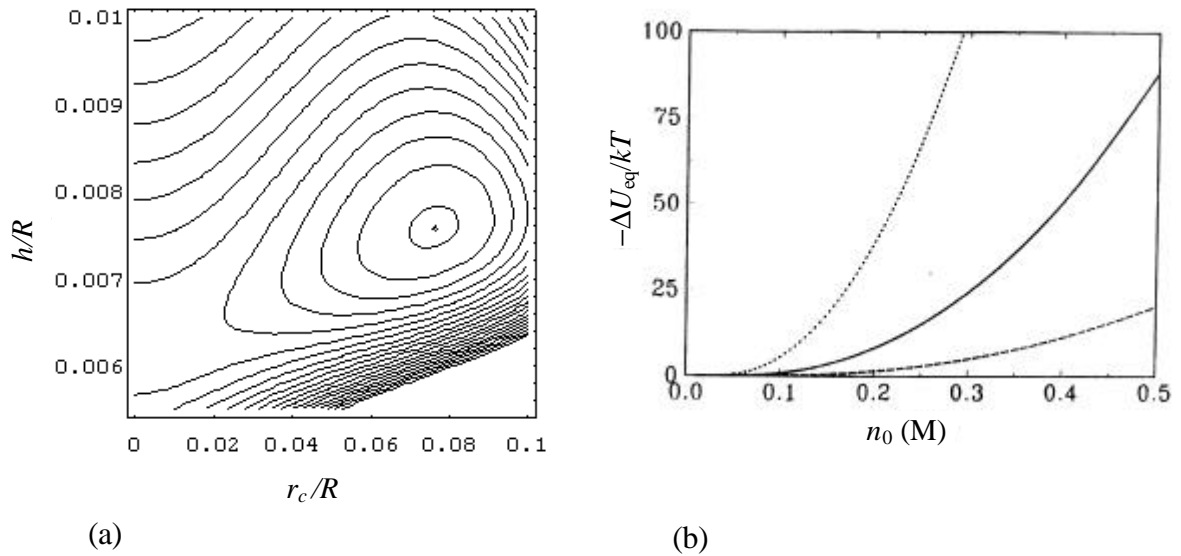
(a)                                                                   (b)

Fig. 6.1. (a) Contour plot of the total drop-drop interaction energy, $U(h,r_c) \equiv U_{vw} + U_{el} + U_{dil}$ for various values of $h/R$ and $r_c/R$, see Fig. 5.19b. The parameter values are: $R = 1$ μm, $y_s = 100$ mV, $s_0 = 1$ mN/m, $n_0 = 0.1$ M, $A_H = 2 \times 10^{-20}$ J. The distance between two neighboring contours equals 2 $kT$; the minimum of the potential surface is $U(h_{eq}, r_{c,eq}) = -60 \, kT$. (b) Plot of $\Delta U_{eq}$ vs. electrolyte concentration $n_0$ for $A_H = 1 \times 10^{-20}$ J and three values of the drop radius: $R = 0.5, 1.0$ and 2.0 μm for the dashed, continuous and dotted line, respectively [4,5].

Let $U(h^*,0)$ be the minimum value of $U$ along the ordinate axis $r_c = 0$ in Fig. 6.1a; the points on this axis correspond to two spherical (non-deformed) drops. Figure 6.1b shows the calculated dependence of $\Delta U_{eq} \equiv U(h_{eq}, r_{c,eq}) - U(h^*,0)$ on the bulk electrolyte concentration $n_0$ for three different values of the drop radius $R$. In fact, $\Delta U_{eq}$ characterizes the gain of energy due to the transition from two interacting *spherical* drops to two *deformed* drops (Fig. 5.19b). This energy gain is due to the interactions of the two drops across the formed film; see the term $pr_c^2 f(h)$ in Eq. (6.1); note that at equilibrium $f(h) < 0$, cf. Eq. (5.10). Figure 6.1b shows that the effect of deformation, characterized by $\Delta U_{eq}$, strongly increases with the rise of $n_0$ and $R$; this can be attributed to suppression of the electrostatic repulsion and enlargement of the contact area.

*Effect of the oscillatory structural force.* Very often the fluid dispersions contain small colloidal particles (such as surfactant micelles or protein globules) in the continuous phase. As described in Section 5.2.7, the presence of these small particles gives rise to an oscillatory structural force, which affects the stability of foam and emulsion films as well as the flocculation processes in various colloids. At higher particle concentrations (volume fractions
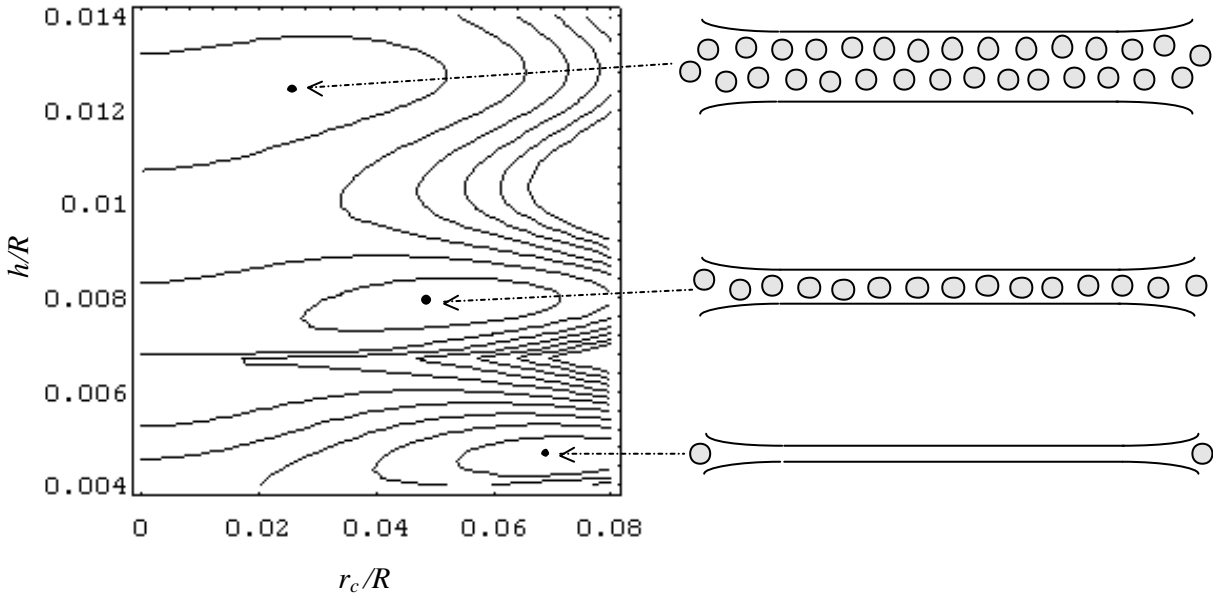
Fig 6.2. Contour plot of the energy, $U(h,r_c) = U_{vw} + U_{el} + U_{dil} + U_{osc}$, between two oil drops of radius $R = 2$ μm in the presence of ionic micelles in water. The parameters correspond to a micellar solution of SNP-25S, see Fig. 5.12: $d = 9.8$ nm, $j = 0.38$, $s = 7.5$ mN/m, $A_H = 5 \times 10^{-21}$ J, $y_s = -135$ mV, $n_0 = 25$ mM, $k^{-1} = 1.91$ nm. The points on the contour plot denote three local minima: $U/kT = -406$; $-140$, and $-37$, corresponding to film containing 0, 1 and 2 micellar layers, respectively [4,5].

above c.a. 15 %) the structural forces stabilize the liquid films and emulsions. At lower particle concentrations the structural forces degenerate into the depletion attraction, which is found to have a destabilizing effect. To quantify the contribution of the oscillatory forces, a respective term, $U_{osc}$, is to be included in the expression for the interaction energy:

$$U(h,r_c) = U_{vw} + U_{el} + U_{dil} + U_{osc} \qquad (6.5)$$

cf. Eq. (6.3). $U_{osc}$ can be calculated by a substitution of $f_{osc}(h)$ from Eq. (5.108) into Eq. (6.1); the other terms in the right-hand side of Eq. (6.5) are determined as explained above.

Figure 6.2 shows a contour plot of $U(h,r_c)$, which is similar to Fig. 6.1a, but computed by means of Eq. (6.5). The oscillatory term $U_{osc}$ leads to the appearance of several local minima separated by "mountain ranges". If the particle volume fraction is smaller than c.a. 10% in the continuous phase, the height of the taller "range" is smaller than $kT$, and it cannot prevent the flocculation of two droplets in the deep *"depletion"* minimum − the deepest minimum (down right in Fig. 6.2). On the other hand, at higher micellar volume fraction these "ranges" become
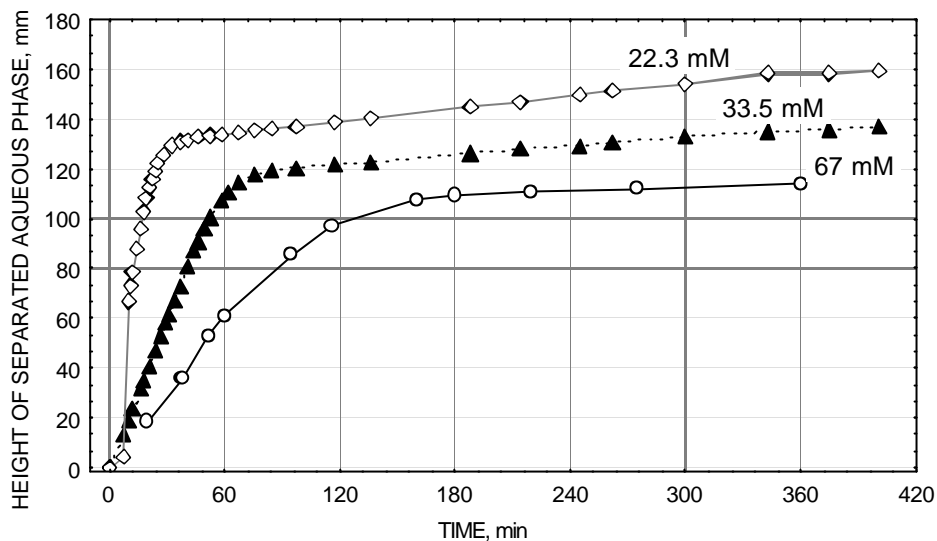
Fig. 6.3. Plot of the height of the water column, separated below a 20% styrene-in-water emulsion, as a function of time. The curves correspond to different surfactant (SNP-25S) concentrations, denoted in the figure, all of them above the CMC [5,6].

taller than $kT$ and act like barriers against the closer approach and flocculation of the two fluid particles. In such case the oscillatory structural forces have a stabilizing effect, which could be a possible explanation of the experimental data shown in Fig. 6.3.

The three curves in Fig. 6.3 correspond to three oil-in-water emulsions containing different concentrations of sodium nonylphenol polyoxyethylene-25 sulfate (SNP25S) in the aqueous phase, viz. 22.3, 33.5 and 67 mM, all of them much above (from 80 to 240 times) the critical micellization concentration, CMC = 0.28 mM. The height of the column of the aqueous phase, below the emulsion cream, is plotted in Fig. 6.3 as a function of time. The cream represents oil drops concentrated below the upper surface of the emulsion owing to the buoyancy force. The initial slope of the curves shows that the rate of water separation diminishes as the surfactant concentration increases. In addition, the more concentrated system finally produces a more *loosely packed* cream (note the positions of the plateaus, Fig. 6.3), possibly due to hampered flocculation. One can attribute the observed effects to the oscillatory structural forces, which impede the flocculation of the emulsion drops and thus decelerate the separation driven by the Archimedes force; see Refs. [5-7] for more details.

In conclusion, we have to mention that for each specified system an estimate should be done to reveal

which of the terms in Eq. (5.53) are predominant, and which of them can be neglected; see also Eqs. (6.3) and (6.5). Similar approach can be applied to describe the multi-droplet interactions in flocs, because in most cases the interaction energy is pair-wise additive. Application of this approach to the description of the kinetics of simultaneous flocculation and coalescence in emulsions can be found in Ref. [8].

### 6.1.2. DEPENDENCE OF THE FILM AREA ON THE SIZE OF DROP/BUBBLE

In Figs. 6.1a and 6.2 the equilibrium position of two attached fluid particles was determined as a minimum of the energy surface $U(h, r_c)$. Alternatively, it is possible to determine the radius, $r_c$, of the equilibrium (or quasi-equilibrium) film with the help of macroscopic force balances.

As an example, let us consider a fluid particle from phase 1, which approaches the boundary between the phases 2 and 3 driven by the buoyancy force; the drop is immersed in the heavier phase 3, see Fig. 6.4. For example, the fluid particle could be an oil drop or air bubble in water. For sufficiently short distance between the fluid particle and the interface a liquid film of uniform thickness $h$ is formed; as a rule, $h$ decreases slowly with time due to a viscous outflow of liquid, until eventually an equilibrium film is formed [9]. The pressures acting on the film surfaces are shown schematically in Fig. 6.4. At equilibrium the net force exerted on the particle should be equal to zero; this yields the following force balance, which is equivalent to Eq. (5.14):

$$\pi r_c^2 P_f = 2\pi r_c \tau \cos\theta + F_b \tag{6.6}$$

$P_2 + P_f$ is the pressure inside the liquid film; $\tau$ is the transversal tension; $\sin\theta \equiv r_c/R_f$ where $R_f$ is the curvature radius of the film surface; $F_b$ is the buoyancy (Archimedes) force, which is equal to the integral of the outer pressure, $P_2(z) = P_2(0) - \Delta\rho g z$, over the surface of the particle:

$$F_b = \mathbf{e}_z \cdot \oint d\mathbf{s}\, P_2(z) = \tfrac{4}{3}\pi R_0^3 \Delta\rho g \; ; \tag{6.7}$$

at the last step, the Gauss–Ostrogradsky theorem has been applied; $z$ is the vertical coordinate; $\Delta\rho$ is the difference between the mass densities of phases 3 and 1; $g$ is the acceleration due to gravity; $R_0$ is the radius of the nondeformed (spherical) fluid particle. The transversal tension $\tau$ accounts for the interaction in the transition zone film-meniscus and is related to the contact
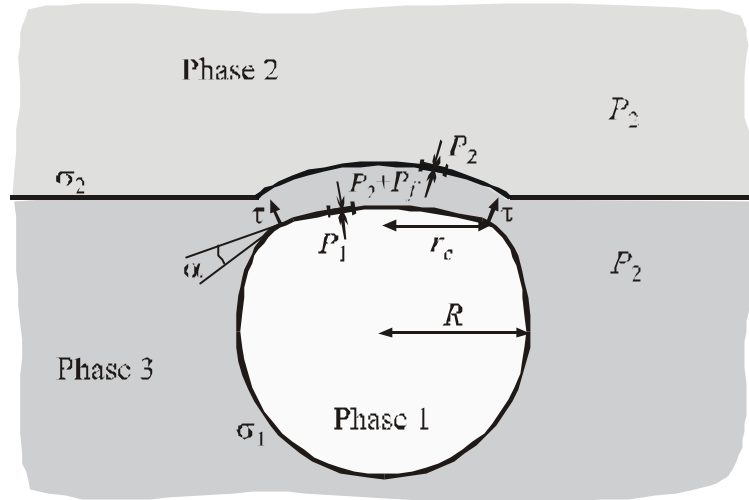
Fig. 6.4. Sketch of a fluid particle from phase 1, which is attached to the boundary between phases 2 and 3; $s_1$ and $s_2$ are the surface tensions of the boundaries 1/3 and 2/3; $t$ is transversal tension. The pressure balances at the two film surfaces illustrate the derivation of Eqs. (6.9) and (6.10).

angle $a$ by Eq. (5.6), viz. $t = s_1 \sin a$; $P_f$ is the excess pressure (with respect to the bulk pressure $P_2$) exerted on the film surface. In general $P_f$ can be presented as a sum of a viscous and a disjoining pressure term:

$$P_f = P_{\text{visc}} + \Pi \tag{6.8}$$

In thick films the disjoining pressure $\Pi$ is negligible, and consequently $P_f \approx P_{\text{visc}}$; in contrast, in thin quasi-equilibrium films the rate of thinning is low, $P_{\text{visc}} \approx 0$ and then $P_f \approx \Pi$. However, at any thickness the Laplace equation is satisfied for the lower and upper film surfaces (Fig. 6.4):

$$\frac{2s_1}{R_f} = P_1 - \left(P_2 + P_f\right) = \Delta P - P_f \tag{6.9}$$

$$\frac{2s_2}{R_f} = \left(P_2 + P_f\right) - P_2 = P_f \tag{6.10}$$

In Eqs. (6.9) and (6.10) the surface tensions of the liquid film are set approximately equal to the surface tensions of the boundaries between the respective bulk phases, $s_1^f \approx s_1$ and $s_2^f \approx s_2$, see Fig. 5.5. The pressure difference, across the drop surface, $\Delta P \equiv P_1 - P_2$, is

$$\frac{2s_1}{R} = \Delta P \tag{6.11}$$

The three equations (6.9), (6.10) and (6.11) form a system for determining the three parameters, $R_f$, $P_f$ and $\Delta P$. The resulting expression for $P_f$ reads

$$P_f = \frac{\overline{s}}{R}, \qquad \text{where} \qquad \overline{s} \equiv \frac{2s_1 s_2}{s_1 + s_2} \qquad (6.12)$$

Next, we substitute Eqs. (6.7) and (6.12) into Eq. (6.6) to obtain

$$p r_c^2 \frac{\overline{s}}{R} - 2p\, r_c t \cos q - \tfrac{4}{3} p R^3 \Delta r\, g = 0 \qquad (6.13)$$

we have set $R \approx R_0$, which is a good approximation in the case of small deformations, that is $(r_c/R)^4 \ll 1$; see Eq. (5.131). The solution of the quadratic equation (6.13) for $r_c$ reads

$$r_c = R \frac{t}{\overline{s}} \cos q + \left( R^2 \frac{t^2}{\overline{s}^2} \cos^2 q + \frac{4\Delta r\, g}{3\overline{s}} R^4 \right)^{1/2} \qquad (6.14)$$

(the other root is physically meaningless). For small contact angles ($t \propto \sin a \ll 1$), Eq. (6.14) reduces to the simpler expression

$$r_c = A R^2, \qquad A \equiv \sqrt{\frac{4\Delta r\, g}{3\overline{s}}} \qquad (6.15)$$

If phases 1 and 2 are *identical fluids*, then $s_1 = s_2 = s$ and Eq. (6.12) yields $\overline{s} = s$. In contrast, if phase 2 is *solid* and we deal with the configuration in Fig. 5.19a, one may set $s_1 = s$, $s_2 \to \infty$, and then Eq. (6.12) yields $\overline{s} = 2s$. Versions of Eq. (6.15) with $\overline{s} = 2s$ have been derived by Derjaguin and Kussakov [10] and Allan et al. [11]. Expression equivalent to Eq. (6.15) follows from the theory of sessile drops/bubbles for zero contact angle measured across the outer phase ($a = 0$); see Ref. [12] and Eq. (31) in Ref. [13].

Equation (6.15) holds irrespective of whether the pressure in the film, $P_f$, is dominated by the viscous pressure $P_{\text{visc}}$ or disjoining pressure $\Pi$. This equation has been derived neglecting the terms with the transversal tension $t$. The effect of $t$ could show up for small drops (bubbles) for which the contribution of the buoyancy force (the term $\propto R^4$ in Eq. 6.14) is vanishing. Hence, a deviation from the dependence $r_c = A R^2$ for small drops could be interpreted as an effect of $t$, see Eq. (6.14), and could serve for determination of the contact angle, $a = \arcsin(t/s)$.
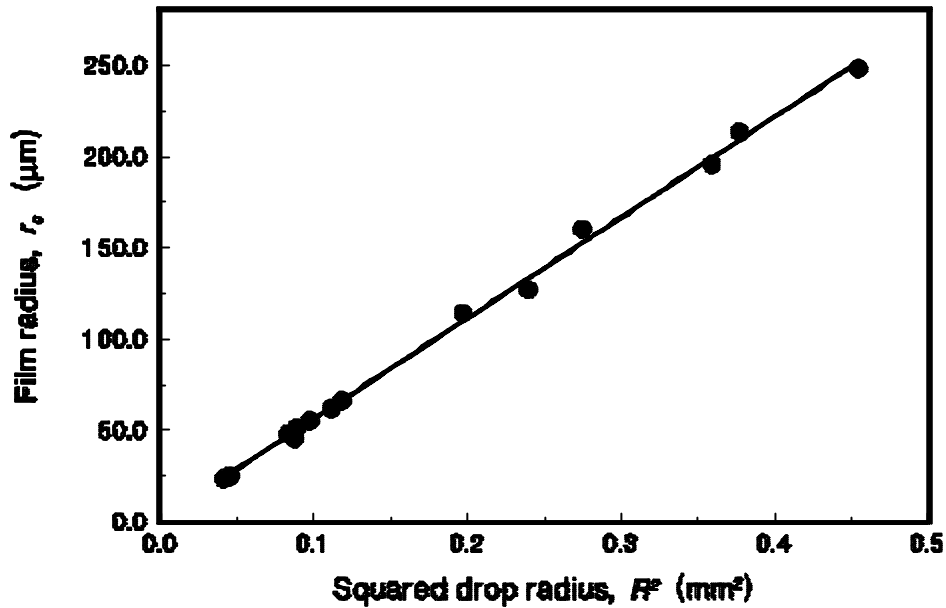
Fig. 6.5. Experimental dependence of the film radius $r_c$ on the "equatorial" radius $R$ of xylene oil drops situated below the phase boundary water–xylene, see Fig. 6.4. The straight line is the best fit with linear regression [14].

In Fig. 6.5 we present experimental data of Basheva [14] for small xylene drops; the system is similar to that in Fig. 6.4 where phases 1 and 2 are of xylene. Phase 3 is a 0.01 M solution of sodium dodecyl sulfate (SDS), preequilibrated with xylene. The data are plotted as $r_c$ vs. $R^2$ in accordance with Eq. (6.15). The density difference between water and xylene is $\Delta r = 0.12$ g/cm$^3$; the interfacial tension xylene − aqueous solution is $s = 5.1$ mN/m. With the latter parameter values from Eq. (6.15) one calculates $A = 5.54$ cm$^{-1}$; on the other hand, the best linear fit of the data in Fig. 6.5 gives a slope $A = 5.52$ cm$^{-1}$. Apparently, there is an excellent agreement between Eq. (6.15) and the experiment. One may check that the experimental data for $r_c$ and $R$, published in tables in Ref. [15], also agree well with Eq. (6.15).

Taking square of Eq. (6.15) and using the expression for the buoyancy force, $F_b = \frac{4}{3} p R^3 \Delta r g$, one obtains [10]:

$$r_c^2 = \frac{R F_b}{p \overline{s}} \qquad (6.16)$$

A generalization of Eq. (6.16) was obtained by Ivanov et al. [16] for two fluid particles (drops,

bubbles) of different radii, $R_1$ and $R_2$, pressed against each other by an external force $F$:

$$r_c^2 = \frac{\overline{R}F}{2p\overline{s}}, \qquad \text{where} \qquad \overline{R} \equiv \frac{2R_1R_2}{R_1+R_2} \qquad (6.17)$$

$\overline{R}$ and $\overline{s}$ can be interpreted as mean diameter and surface tension, see also Eq. (6.12). If one of the two drops is a semiinfinite liquid phase, then $R_2 \rightarrow \infty$, $R_1 = R$, $\overline{R} = 2R$ and Eq. (6.17) reduces to Eq. (6.16). The latter two equations have found applications in the studies of the hydrodynamic interactions of emulsion drops (see Fig. 6.6 below).

## 6.2.    HYDRODYNAMIC INTERACTIONS

The motion of a colloidal particle toward an interface (or another particle) is always affected by the viscous drag force. The strongest viscous dissipation of energy happens in the narrow zone of collision, where the two surfaces approach close to each other. The friction, accompanying the expulsion of the liquid from the collision zone, can cause a local deformation of fluid particles (gas bubbles, emulsion droplets or lipid vesicles), see e.g. Ref. [9]. The present section is devoted to such *hydrodynamic interactions* which are related to the viscous friction. We review the most useful theoretical expressions. One could find additional information in the comprehensive treatises on hydrodynamic interactions, Refs. [5, 9, 17-22].

    *Stokes regime of particle motion.* At comparatively large surface-to-surface separations a spherical particle, moving under the action of a total driving force $F$, will obey the known Stokes equation for the velocity, see e.g. Ref. [23],

$$V_{St} = \frac{F}{6p h R} , \qquad (6.18)$$

where $h$ is the dynamic viscosity of the liquid medium, and $R$ is the radius of the particle. Equation (6.18) is obeyed not only by solid beads, but also by small (spherical) drops and bubbles in the presence of surfactant dissolved in the liquid medium. The role of surfactant, even at comparatively low concentrations, is to render the surface of the fluid particle tangentially immobile owing to the formation of a dense adsorption monolayer.

### 6.2.1. *TAYLOR REGIME OF PARTICLE APPROACH*

At shorter distance between a spherical particle and an interface (or another particle) the hydrodynamic interaction between them becomes significant. This results in a dependence of the velocity of mutual approach on the surface-to-surface distance, $h$. For $h/R \ll 1$ the latter dependence is given by the *Taylor* formula [24] for the velocity:

$$V_{\mathrm{Ta}} = \frac{2hF}{3\pi\eta R^2} = V_{\mathrm{St}}\frac{4h}{R} \; . \tag{6.19}$$

Since $h/R \ll 1$, it follows that $V_{\mathrm{Ta}} \ll V_{\mathrm{St}}$, i.e. the velocity of mutual approach is considerably decreased by the hydrodynamic interactions. Note that Eq. (6.19) is valid for two *identical* spheres of radius $R$. This equation can be generalized for two spheres of *different* radii, $R_1$ and $R_2$ [18]:

$$V_{\mathrm{Ta}} = \frac{2hF}{3\pi\eta\overline{R}^2} \tag{6.20}$$

where $\overline{R}$ is defined by Eq. (6.17). In the limit of two identical spheres ($R_1 = R_2 = R$) one has $\overline{R} = R$, whereas for the interaction of a spherical particle with a planar interface ($R_1 = R$, $R_2 \to \infty$) one obtains $\overline{R} = 2R$. In general, the total force acting on the particle, $F$, can be expressed as a sum of some external driving force, $F_E$, and the surface force $F_S$:

$$F = F_E - F_S, \qquad\qquad F_S \equiv -\frac{dU(h)}{dh} \tag{6.21}$$

where $U$ is defined by Eq. (5.53). The opposite signs of $F_E$ and $F_S$ stem from the convention, that the "external" force $F_E$ pushes the particle toward the interface (the other particle), whereas a repulsive "surface" force, $F_S > 0$, opposes the thinning of the gap. (Attractive surface force, $F_S < 0$, is also possible.) The *external* force $F_E$ can be the gravitational, buoyancy or Brownian force. The time of mutual approach of two particles (the drainage time of a liquid film) is [18]

$$t_a = \int_0^{h_A} \frac{dh}{V(h)} \tag{6.22}$$

where $V$ denotes velocity and $h_A$ is some initial value of the surface-to-surface distance. For constant

$F$, the substitution of $V_{Ta} \propto h$ for $V(h)$ in Eq. (6.22) yields $t_a \to \infty$, i.e. infinitely long time is needed for the two surfaces to come into direct contact. On the other hand, if the force at short distances is dominated by the van der Waals interaction, then in view of Eqs. (5.61) and (6.21) $F \approx F_S \propto 1/h^2$, $V_{Ta} \propto 1/h$, and Eq. (6.22) gives a finite value for the time of approach $\boldsymbol{t}_a$.

### 6.2.2. *INVERSION THICKNESS FOR FLUID PARTICLES*

Two fluid particles (drops, bubbles) approaching each other are initially spherical. With the decrease of the distance between them, the interfacial shape in the gap changes from convex to concave. The thickness corresponding to this inversion of the sign of the interfacial curvature is called the *inversion thickness*, $h_{inv}$. From a physical viewpoint this is the beginning of the deformation of the droplets (bubbles) in the contact zone, with subsequent formation of a thin film between them (see Fig. 5.19). One can estimate the inversion thickness from the following expression [18, 25, 26]

$$h_{inv} \approx \frac{F}{2\boldsymbol{p}\overline{\boldsymbol{s}}} \; , \tag{6.23}$$

where $\overline{\boldsymbol{s}}$ is related to the interfacial tensions of the two fluid particles, $\boldsymbol{s}_1$ and $\boldsymbol{s}_2$, by means of Eq. (6.12). If one of the particles is solid ($\boldsymbol{s}_1 \to \infty$, $\boldsymbol{s}_2 = \boldsymbol{s}$), then $\overline{\boldsymbol{s}} = 2\boldsymbol{s}$. Equation (6.23) is valid for relatively large surface-to-surface distances between the two drops, for which the surface forces can be neglected ($F \approx F_E$). A generalization of Eq. (6.23), taking into account the effects of the surface forces and the particle size, was reported in Ref. [27]:

$$h_{inv} = \frac{F}{2\boldsymbol{p}\overline{\boldsymbol{s}}} + \frac{\overline{R}}{2\overline{\boldsymbol{s}}} h_{inv} \Pi(h_{inv}) \; ; \tag{6.24}$$

as usual, $\Pi(h)$ is disjoining pressure. In general, Eq. (6.24) holds for two dissimilar droplets of radii $R_1$ and $R_2$, and surface tensions $\boldsymbol{s}_1$ and $\boldsymbol{s}_2$; see Eqs. (6.12) and (6.17). One can determine $h_{inv}$ by numerical solution of Eq. (6.24) if the dependencies $\Pi(h)$ and $F(h)$ are given, see e.g. Ref. [5].

### 6.2.3. *REYNOLDS REGIME OF PARTICLE APPROACH*

For $h < h_{inv}$ a liquid film is formed in the zone of contact of the two surfaces (Fig. 5.19). The viscous dissipation of energy in this film is strong enough to dominate the net hydrodynamic force. In such case

the rate of approach of two fluid particles obeys the Reynolds formula, which describes the rate of thinning of a planar film between two solid discs [28, 23]:

$$V_{\text{Re}} = \frac{2h^3 F}{3\boldsymbol{p}\boldsymbol{h}r_c^4}$$

(6.25)

$h$ is the distance between the discs (the film thickness), $r_c$ is the radius of the disc (film) radius. In the case of fluid particles $r_c$ can be estimated from Eqs. (6.14)–(6.17).

Since $V_{\text{Re}} = dh/dt$, by integration of Eq. (6.25) one can deduce an expression for the time needed to bring two parallel discs (the two film surfaces) from an initial separation $h_1$ to a final separation $h_2$ under the action of a *constant* force $F$:

$$t = \frac{3\boldsymbol{p}\boldsymbol{h}r_c^4}{4F}\left(\frac{1}{h_2^2} - \frac{1}{h_1^2}\right)$$

(6.26)

The latter equation was derived by Stefan [29] in 1874. One can combine Eqs. (6.25) and (6.17) to obtain [5]:

$$V_{\text{Re}} = \frac{8\boldsymbol{p}\overline{\boldsymbol{s}}^{-2}h^3}{3\boldsymbol{h}\overline{R}^2 F}$$

(6.27)

It is interesting to note, that in *Reynolds* regime (in which there is flattening and Eq. 6.27 holds) the velocity $V_{\text{Re}}$ *decreases* with the rise of the driving force $F$. This tendency is exactly the opposite to that for the particle motion in *Stokes* or *Taylor* regimes, cf. Eqs. (6.18) and (6.20). The latter fact leads to a non-monotonic dependence of the droplet life-time, $\boldsymbol{t}_a$, on the drop radius $R$; see Fig. 6.6 below.

### 6.2.4. *TRANSITION FROM TAYLOR TO REYNOLDS REGIME*

It is possible to describe smoothly the transition from Taylor to Reynolds regime, i.e. the transition from spherical to deformed fluid particles. The following generalized expression was derived in Ref. [30]:

$$F = \frac{3}{2} p h V \frac{\overline{R}^2}{h} \left( 1 + \frac{r_c^2}{h\overline{R}} + \frac{r_c^4}{h^2 \overline{R}^2} \right) \tag{6.28}$$

where $\overline{R}$ is defined by Eq. (6.17). For small film radii, $r_c \to 0$, Eq. (6.28) reduces to the Taylor's Eq. (6.20), whereas for large films, $r_c^2/(h\overline{R}) \gg 1$, Eq. (6.28) yields the Reynolds' Eq. (6.25). Expressing the velocity from Eq. (6.28) one obtains [5]

$$\frac{1}{V} = \frac{1}{V_{\mathrm{Ta}}} + \frac{1}{\sqrt{V_{\mathrm{Ta}} V_{\mathrm{Re}}}} + \frac{1}{V_{\mathrm{Re}}} \tag{6.29}$$

To calculate the life time of a doublet from two emulsion drops moving towards each other under the action of a *constant* force $F$ one can use the expression [5]

$$t_a = \int_{h_{\mathrm{cr}}}^{h_A} \frac{dh}{V(h)} = \frac{3 p h \overline{R}^2}{2F} \left[ \ln \frac{h_A}{h_{\mathrm{cr}}} + \frac{r_c^2}{h_{\mathrm{cr}} \overline{R}} \left( 1 - \frac{h_{\mathrm{cr}}}{h_A} \right) + \frac{r_c^4}{2 h_{\mathrm{cr}}^2 \overline{R}^2} \left( 1 - \frac{h_{\mathrm{cr}}^2}{h_A^2} \right) \right] \tag{6.30}$$

which is derived by integration of Eq. (6.28); $h_{\mathrm{cr}}$ denotes the critical thickness of rupture of the liquid film; as before, $h_A$ is an initial thickness of the film.

In the case of coalescence of an oil drop with its homophase (oil drop below a flat oil-water interface, see Fig. 5.19a) one has $\overline{R} = 2R$, where $R$ is the radius of the drop, which experiences a buoyancy force $F_b = \frac{4}{3} p R^3 g \Delta r$, with $g$ and $\Delta r$ being the gravity acceleration and the density difference. Setting $F \approx F_b$, and combining Eqs. (6.16) and (6.30), one can calculate the dependence $t_a = t_a(R)$ if an estimate for the critical thickness, $h_{\mathrm{cr}}$, is available; see Eq. (6.36) below. The calculations show that the curves of $t_a$ vs. $R$ should exhibit a minimum in the region $R = 10 - 200$ μm.

To check the predictions of the theory experiments with soybean oil droplets in aqueous solution of the protein bovine serum albumin (BSA) have been carried out by Basheva et al. [31]. The oil drops of various size have been released by means of a syringe in the aqueous solution; then the drops move upwards under the action of the buoyancy force and approach a horizontal oil−water interface. The life-time $t_a$ of the drops beneath the interface was measured as a function of the drop radius, $R$. The data are presented in Fig. 6.6. The theoretical curve is calculated by means of Eqs. (6.16) and (6.30). For all drops $h_A = 15$ μm was used.
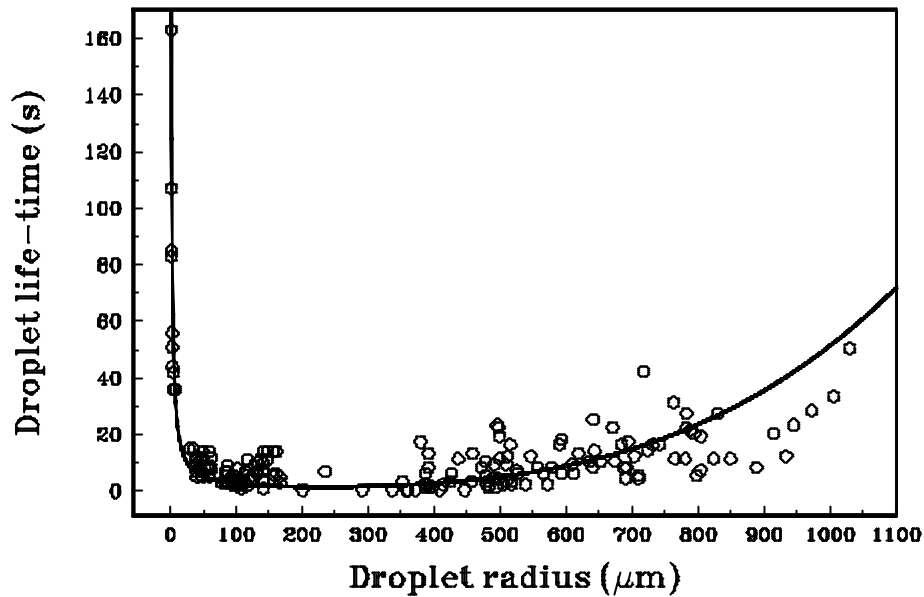
Fig. 6.6. Lifetime $t_a$ plotted versus the radius, $R$, of oil-in-water drops approaching from below the water–oil interface. The circles are experimental points for aqueous solutions of bovine serum albumin (BSA) with 0.15 M NaCl; the oil phase is soybean oil [31]. The theoretical curve is drawn by means of Eqs. (6.16) and (6.30).

The arbitrariness of this choice does not affect substantially the results for $t_a$. The critical thickness, $h_{cr}$, was calculated by means of Eq. (24) in Ref. [5] assuming predominant van der Waals forces in the film. One sees in Fig. 6.6 that the theory agrees well with the experiment. The left branch of the curve corresponds to the Taylor regime (non-deformed droplets), whereas the right branch corresponds to the Reynolds regime (planar film between the droplets); for details see Refs. [5, 31].

### 6.2.5. *FLUID PARTICLES OF COMPLETELY MOBILE SURFACES (NO SURFACTANTS)*

If the surface of an emulsion droplet is mobile, it can transmit the motion of the outer fluid to the fluid within the droplet. This leads to a circulation pattern of the inner fluid and affects the dissipation of energy in the system. The problem about the approach of *two nondeformed (spherical)* drops or bubbles in the absence of surfactants has been investigated by many authors [32-41] and a number of solutions, generalizing the Taylor equation (6.20), have been obtained. For example, the velocity of central approach of two spherical drops in pure liquid, $V_p$, is related to the total force, $F$, by means of a Padé-type expression derived by Davis et al. [40]

$$V_p = V_{Ta} \frac{1 + 1.711x + 0.461x^2}{1 + 0.402x}, \qquad x = \frac{h_{out}}{h_{in}} \sqrt{\frac{\overline{R}}{2h}} \qquad (6.31)$$

where, as usual, $h$ is the closest surface-to-surface distance between the two drops; $h_{in}$ and $h_{out}$ are the viscosities of the liquids inside and outside the droplets. In the limiting case of solid particles one has $h_{in} \rightarrow \infty$ and Eq. (6.31) reduces to the Taylor equation, Eq. (6.20). In the case of *close* approach of two drops ($h \rightarrow 0$ and $x \gg 1$) the velocity $V_p$ is proportional to $\sqrt{h}$. Consequently, the integral in Eq. (6.22) is convergent and the two drops can come into contact ($h = 0$) in a finite period of time ($t_a < \infty$) under the action of constant force $F$. In contrast, in the case of immobile interface ($h_{in} \rightarrow \infty$ and $x \ll 1$) one has $V_{Ta} \propto h$ and $t_a \rightarrow \infty$ for $F = $ const.

In the limiting case of two spherical *gas bubbles* ($h_{in} \rightarrow 0$) in pure liquid, Eq. (6.31) cannot be used; instead, $V_p$ can be calculated from the expression due to Beshkov et al. [37]

$$V_p = \frac{F}{2p h_{out} \overline{R} \ln\left(\overline{R}/h\right)} \qquad (6.32)$$

Note that in this case $V_p \propto (\ln h)^{-1}$ and the integral in Eq. (6.22) is convergent, that is the hydrodynamic theory predicts a *finite* lifetime of a doublet of two colliding spherical bubbles in pure liquid. Of course, the real lifetime of a doublet of bubbles or drops is affected by the surface forces for $h < 100$ nm, which should be accounted for in $F$, see Eq. (6.21); this may lead to the formation of a thin film in the zone of contact, as discussed above.

### 6.2.6. *FLUID PARTICLES WITH PARTIALLY MOBILE SURFACES (SURFACTANT IN CONTINUOUS PHASE)*

The presence of surfactant in the continuous phase and at the surface of fluid particles decreases their surface mobility. This is due mostly to the effect of Gibbs elasticity, $E_G$, which leads to the appearance of surface tension gradients (Marangoni effect). The latter oppose the viscous stresses due to the hydrodynamic flow and suppress the two-dimensional flow throughout the phase boundary. In the limit $E_G \rightarrow 0$ the interface becomes tangentially immobile. When the effect of the driving force $F$ is small compared to that of the capillary pressure of the droplets/bubbles, the deformation of the two spherical fluid particles upon collision is only a small perturbation in the zone of contact. Then the film

thickness and the pressure within the gap can be presented as a sum of a non-perturbed part and a small perturbation. Solving the resulting linearized hydrodynamic problem for negligible interfacial viscosity, an analytical formula for the velocity of approach was derived by Ivanov et al. [16]:

$$\frac{V}{V_{\mathrm{Ta}}} = \frac{h_s}{2h}\left[\frac{d+1}{d}\ln(d+1)-1\right]^{-1} \tag{6.33}$$

where, as usual, $V_{\mathrm{Ta}}$ is the Taylor velocity given by Eq. (6.20); the dimensionless parameter $d$ and the characteristic surface diffusion thickness $h_s$ are defined as follows

$$d \equiv \frac{h_s}{h(1+b)} \;, \qquad h_s \equiv \frac{6h_{\mathrm{out}}D_s}{E_G} \;, \qquad b \equiv \frac{3h_{\mathrm{out}}D}{E_G}\left(\frac{\partial c}{\partial \Gamma}\right)_{\mathrm{eq}} = \frac{3h_{\mathrm{out}}D}{\Gamma}\left(\frac{\partial c}{\partial s}\right)_{\mathrm{eq}} \tag{6.34}$$

and $D$ denotes the bulk diffusivity of the surfactant (dissolved in the continuous phase); $D_s$ is its surface diffusivity; as before, $s$ and $E_G$ are the surface tension and surface (Gibbs) elasticity, $c$ and $\Gamma$ are surfactant concentration and adsorption; the subscript "eq" denotes equilibrium values. In the limiting case of very large $E_G$ (tangentially immobile interface) the parameter $d$ tends to zero and one can verify that Eq. (6.33) predicts $V \to V_{\mathrm{Ta}}$, as it should be expected.

Equation (6.33) is applicable when the surfactant is dissolved in the continuous phase. In contrast, if the surfactant is dissolved in the emulsion-drop phase, it can efficiently saturate the drop surface and to suppress the effect of surface elasticity [42, 43]. In such case, the drop surface behaves as almost completely mobile and one could apply Eq. (6.31) to estimate the velocity of approach [5]. The relative solubility of the surfactant in the water and oil phases is characterized by the hydrophile-lipophile balance (HLB) − see the book by Krugljakov [44].

### 6.2.7. CRITICAL THICKNESS OF A LIQUID FILM

The surface of a fluid particle is corrugated by capillary waves due to thermal fluctuations or other perturbations. The interfacial shape can be expressed mathematically as a superposition of Fourier components with different wave numbers and amplitudes. If attractive disjoining pressure is present, it enhances the amplitude of corrugations in the zone of contact of two droplets (Fig. 5.19) [45-48]. For *every* Fourier component there is a film thickness, called transitional thickness, $h_{\mathrm{tr}}$, at which *the respective* surface fluctuation becomes unstable and this surface corrugation begins to grow

spontaneously [18, 26]. For $h_{tr} > h > h_{cr}$ the film continues to thin, while the instabilities grow, until the film ruptures at a certain critical thickness $h = h_{cr}$. The transitional thickness of the film between two deformed drops (Fig. 5.19b) can be computed solving the following transcendental equation [5, 27]:

$$\frac{2+d}{1+d} = \frac{h_{tr}r_c^2[\Pi'(h_{tr})]^2}{8\overline{s}\left[2\overline{s}/\overline{R}-\Pi(h_{tr})\right]}\,, \qquad \qquad \Pi' \equiv \frac{\partial\Pi}{\partial h} \tag{6.35}$$

As before, $r_c$ denotes the radius of the film formed between the two fluid particles. The effect of surface mobility is characterized by the parameter $d$, see Eq. (6.34); note that $d$ depends on $h_{tr}$, viz. $d = (h_s/h_{tr})/(1 + b)$; for tangentially immobile interfaces $h_s \to 0$ and hence $d \to 0$. In addition, Eq. (6.35) shows that the disjoining pressure significantly influences the transitional thickness $h_{tr}$; this equation is valid for $\Pi < 2\overline{s}/\overline{R}$, i.e. for a film which thins and ruptures before reaching its equilibrium thickness, corresponding to $\Pi = P_c = 2\overline{s}/\overline{R}$; see. Eq. (5.1). The calculation of the transitional thickness $h_{tr}$ is a prerequisite for computing the critical thickness $h_{cr}$. For the case of two *identical* attached fluid particles of surface tension $s$ and radius $R$ (Fig. 5.19b) the critical thickness can be obtained as a solution of the equation [48, 49]

$$h_{cr}^2 = \frac{2kT}{I(h_{cr},h_{tr})}\exp\left[\frac{I(h_{cr},h_{tr})}{4s}\right] \tag{6.36}$$

where $I(h_{tr},h_{cr})$ stands for the following function

$$I(h_{cr},h_{tr}) = \Pi'(h_{tr})r^2\int\limits_{h_{cr}}^{h_{tr}}\frac{\Pi'\,dh}{\Phi_v(h)[2s/R-\Pi(h)]} \tag{6.37}$$

Here $\Phi_v$ is a *mobility factor* accounting for the tangential mobility of the surface of the fluid particle; expressions for $\Phi_v$ can be found in Ref. [22]. In the special case of tangentially immobile interfaces and large film (negligible effect of the transition zone) one has $\Phi_v(h) \equiv 1$; then the integration in Eq. (6.37) can be carried out analytically [48, 49]:

$$I(h_{cr},h_{tr}) = \Pi'(h_{tr})r^2\ln\left[\frac{2s/R-\Pi(h_{cr})}{2s/R-\Pi(h_{tr})}\right] \tag{6.38}$$

Equations (6.35)−(6.38) hold for an emulsion film formed between two attached liquid drops, and for a foam film intervening between two gas bubbles. In Fig. 6.7 we compare the prediction of Eqs. (6.35)−(6.38) with experimental data for $h_{cr}$ vs. $r_c$, obtained by Manev et al. [50] for free foam films formed from aqueous solution of 0.43 mM SDS + 0.1 M NaCl.
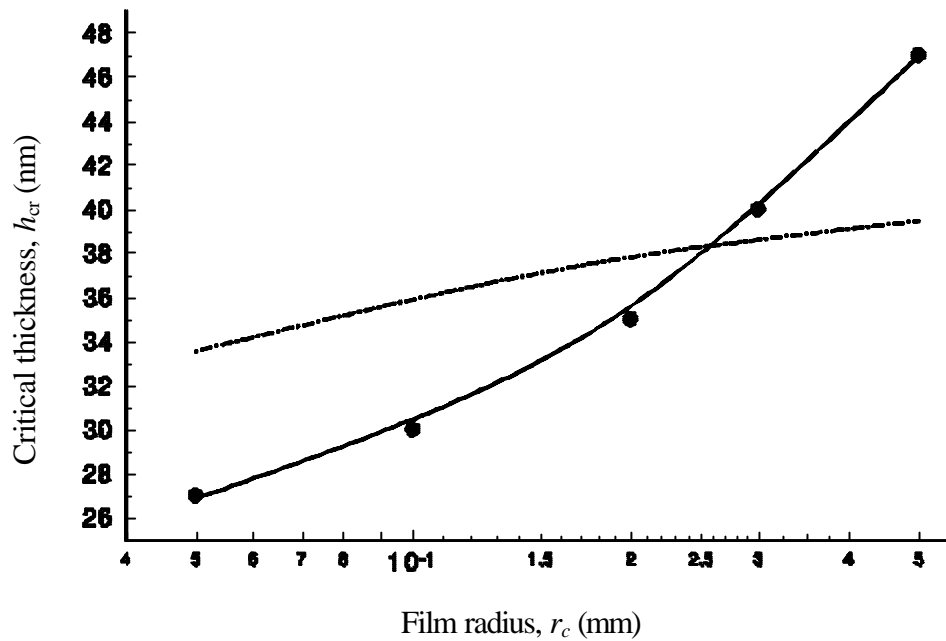
Fig. 6.7. Critical thickness, $h_{cr}$, vs. radius, $r_c$, of a foam film formed from aqueous solution of 0.43 mM SDS + 0.1 M NaCl: comparison between experimental points, measured by Manev et al. [50], with the theoretical model based on Eqs. (6.35)-(6.38) − the solid line; no adjustable parameters. The dot-dashed line shows the best fit obtained using the simplifying assumptions that $h_{cr} \approx h_{tr}$ and that the electromagnetic retardation effect is negligible.

It turns out that for this system the solution–air surface behaves as tangentially immobile, and then $\Phi_v \equiv 1$, see Ref. [22]. The disjoining pressure was attributed to the van der Waals attraction: $\Pi = -A_H/(6\pi h^3)$, where $A_H$ was calculated with the help of Eq. (5.75) to take into account the electromagnetic retardation effect.

The solid line in Fig. 6.7 was calculated by means of Eqs. (6.35)–(6.38) *without* using any adjustable parameters; one sees that there is an excellent agreement between this theoretical model and the experiment [22]. The dot-dashed line in Fig. 6.7 shows the best fit obtained if the retardation effect is neglected ($A_H$ = const.) and if the critical thickness is approximately identified with the transitional thickness ($h_{cr} \approx h_{tr}$), cf. Ref. [51]. The difference between the two fits shows that the latter two effects are essential and should not be neglected. In particular, the retardation effect turns out to be important in the experimental range of critical thicknesses, which is 25 nm $< h_{cr} <$ 50 nm in this specific case.

**6.3.    DETACHMENT OF OIL DROPS FROM A SOLID SURFACE**

The subject of this section is the detachment of oil drops from a solid substrate by *mechanical* and *physicochemical* factors, such as shear flow in the adjacent aqueous phase and modification of the interfaces due to adsorption of surfactants. These processes have practical importance for enhanced oil recovery [52, 53], detergency [54] and membrane emulsification [55-57]. Analogous experiments on deformation and detachment in shear flow have been carried our to explore the mechanical properties of biological cells and their adhesion to substrates [58, 59]. Despite its importance, the drop detachment has been investigated only in few studies. Our purpose here is to briefly review the available works, to systematize and discuss the accumulated information and to indicate some non-resolved research problems.

*6.3.1.    DETACHMENT OF DROPS EXPOSED TO SHEAR FLOW*

The detachment of *solid* colloidal particles from a flat surface (substrate) is studied better than the analogous problem for liquid drops. Hydrodynamic flows normal and parallel to the substrate were considered. The incipient motion of a detaching particle can be described as a superposition of three modes: sliding, rolling and lifting. Expressions for the hydrodynamic force and torque acting on an attached spherical particle were derived. The comparison of the computed and experimentally measured critical hydrodynamic force for particle release show a good agreement, indicating that the essential physics of the problem has been captured in the model; for details see the studies by Hubbe [60], Sharma et al. [61], and the literature cited therein.

What concerns the more complicated problem about the detachment of *liquid* drops from substrates, specific theoretical difficulties arise from the deformability of the drops and from the boundary conditions at the three-phase contact line. Technologically motivated studies [62, 63] established linkages between the value of the interfacial tension and the removal of oil drops. Thompson [54] examined experimentally the effects of the oil-water interfacial tension and the three-phase contact angle on the efficiency of washing of fabrics; in that study the mechanism of oil detachment was not directly observed.

Mahé et al. [64-66] investigated experimentally the detachment of alkane drops from a glass substrate by shear flow in the aqueous phase. According to them, a liquid drop detaches when the exerted hydrodynamic drag equals the maximum retentive capillary force (the integral of the oil-water surface tension along the contact line) [64]. The hydrodynamic drag force, $F_H$, was estimated by means of a formula due to Goldman et al. [67]:

$$F_H \propto \boldsymbol{h}\hat{\boldsymbol{g}}\,R^2 \tag{6.39}$$

where $\boldsymbol{h}$ is the viscosity of the continuous (water) phase; $R$ is the radius of the oil droplet; $\hat{\boldsymbol{g}} \equiv \partial v_x/\partial z$ characterizes the rate of the applied shear flow (the $x$ and $z$ axes are oriented, respectively, tangential and normal to the substrate). On the other hand, the adhesion force $F_A$ has been evaluated by means of a formula derived by Dussan and Chow [68]:

$$F_A = \boldsymbol{s}L(\cos\boldsymbol{q}_A - \cos\boldsymbol{q}_R) \tag{6.40}$$

where $L$ is the width of the drop, $\boldsymbol{q}_A$ and $\boldsymbol{q}_R$ are the *advancing* and *receding* contact angles (see Fig. 6.9 below); as usual, $\boldsymbol{s}$ is the interfacial tension. According to Mahé et al., the critical shear rate, $\hat{\boldsymbol{g}}_c$, corresponds to

$$F_H = F_A \qquad \text{(integral criterion for drop detachment)} \tag{6.41}$$

Equating (6.39) and (6.40) and setting $L \propto r_c$ one obtains [64]

$$\hat{\boldsymbol{g}}_c\,R^2 \propto \boldsymbol{s}\,\frac{r_c}{\boldsymbol{h}}\,(\cos\boldsymbol{q}_A - \cos\boldsymbol{q}_R) \tag{6.42}$$

As usual, $r_c$ is the radius of the contact line, see Fig. 5.19a. Experimental plots of $\hat{\boldsymbol{g}}_c\,R^2$ vs. $r_c$ showed a good linear dependence [64, 66], as predicted by Eq. (6.42). This theoretical modeling seems adequate; note however, that it has not yet been proven whether or not the slopes of the experimental straight lines are proportional to $\boldsymbol{s}\,(\cos\boldsymbol{q}_A - \cos\boldsymbol{q}_R)/\boldsymbol{h}$.

For the time being, the *"integral"* criterion for drop detachment, Eq. (6.41), is a hypothesis, whose validity needs additional experimental proofs. There is neither detailed theoretical model, nor systematic experimental data about the detachment of oil drops in tangential shear flow (note that the studies by Mahé et al. are focused mostly on attachment, rather than on detachment, of drops). Moreover, there could be an alternative *"local"* criterion for detachment

## EMULSIFICATION MECHANISM
### (Destabilization of the Oil-Water Interface)



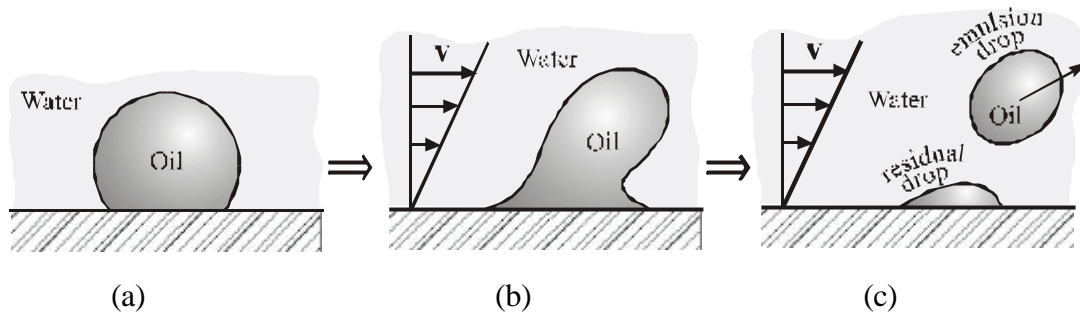(a)                                (b)                                (c)

Fig. 6.8. Scheme of the emulsification mechanism of oil-drop detachment by a shear flow. (a) An oil drop attached to the boundary water-solid. (b) If shear flow is present in the water phase, the hydrodynamic drag force deforms the drop, which could acquire unstable shape and (c) could be split on two parts: residual and emulsion drop, the latter being drawn by the flow away.

of the drop (related to a local violation of the Young equation), which is discussed below.

Basu et al. [69] described theoretically the sliding of an oil drop along a solid surface in shear flow. This is a special pattern of motion of an already detached drop; however the mechanism and criteria of detachment have not been investigated in Ref. [69].

It should be noted that from a theoretical viewpoint the drop detachment from a solid substrate resembles the hydrodynamic problem for sliding of a liquid drop down an inclined plate [68, 70-73]. Another, related problem is the detachment of emulsion drops from the orifices of pores; this is a central issue in the method of emulsification by means of microporous glass and ceramic membranes, which has found various practical applications [55-57].

*Hydrodynamic mechanisms of drop detachment*. Based on the preceding studies one may conclude that two major hydrodynamic mechanisms for detachment of a liquid drop from a solid substrate by a shear flow can be distinguished [54]:

(a) *Emulsification mechanism* due to destabilization of the *oil-water interface*;

(b) *Rolling-up mechanism* related to destabilization of the *three-phase contact line*.

*(a) The emulsification mechanism* (Fig. 6.8) involves a deformation of the attached oil drop by the shear flow until a unstable configuration is reached. Then the oil drop splits into an *emulsion*

*drop* convected by the shear flow, and a *residual drop*, which remains attached to the substrate. Lower oil-water interfacial tension and greater contact angle (measured across the oil phase) are found to facilitate the drop detachment by emulsification. At our best knowledge, the emulsification mechanism, termed also the *"necking and drawing"* mechanism, was first explicitly formulated by Dillan et al. [62].

   *(b) The rolling-up mechanism*, as a disbalance of the interfacial tensions acting at the three-phase contact line, was proposed by Adam [74] long ago. This mechanism is related to the notion of *advancing* and *receding* contact angle. Let $q$ be the contact angle measured across the oil. If oil is added to a quiescent oil drop, its volume and contact angle increase until a threshold value, the *static advancing* angle $q = q_?$, is reached (Fig. 6.9a). Then the contact line begins to expand and the oil spreads over the solid; usually the *dynamic* advancing angle, $q_A^{(d)}$, is smaller than the threshold static advancing angle, $q_A$. In this aspect, there is an analogy with *static friction* (body dragged over a surface). Moreover, some theoretical studies attribute the hysteresis of contact angle to static friction [71, 72].

Likewise, if oil is sucked out from a quiescent oil drop, its volume and contact angle decrease until a threshold value $q = q_R$, the *static receding* angle, is reached (Fig. 6.9b). Then the contact line begins to shrink; usually the *dynamic* receding angle, $q_R^{(d)}$, is larger than the threshold static receding angle, $q_R$; again there is an analogy with static friction. The *hysteresis* of the contact angle consists in the fact that for quiescent drops $q_R \leq q \leq q_A$.
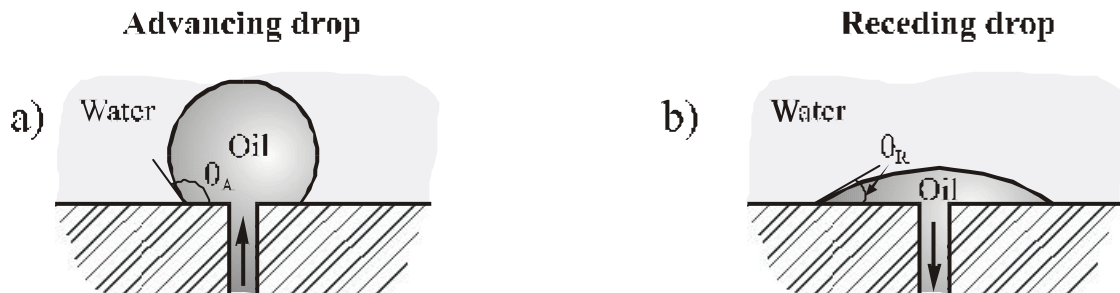


Fig. 6.9. (a) The static advancing angle $q_A$ is the threshold value of the contact angle just before the advance of the contact line. (b) The static receding angle $q_R$ is the threshold value of the contact angle just before the receding of the contact line.
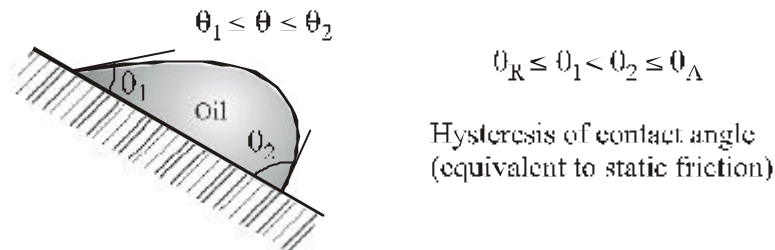
## Static drop on inclined plane



Fig. 6.10 An immobile liquid drop over an inclined plate.

A liquid drop is able to rest over an *inclined plate* owing to the fact that the contact angle can vary along the contact line [70]; in general, $q_1 \leq q \leq q_2$, see Fig. 6.10. The necessary condition the contact line to be immobile is $q_R \leq q_1 < q_2 \leq q_A$.

Similarly, if a liquid drop is exposed to a *shear flow* (Fig. 6.11a), the contact line will be immobile if $q_R \leq q_1 < q_2 \leq q_A$.

If we have $q_2 > q_A$ at the leeward side of the drop, Fig. 6.11b, the contact line will advance in this zone and the oil-wet area will increase, i.e. the shear will produce a spreading of the oil drop (rather than detachment).

If $q_A \to 180°$, then the contact line at the leeward zone remains immobile, but the deformed oil drop could form a water film in this zone, Fig. 6.11c. Such events have been observed by Mahé et al. [64].
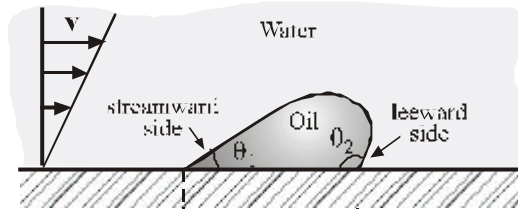
When the magnitude of the shear increases, the contact angle $q_1$ at the stream-ward edge of the drop decreases. At the instant when $q_1 = q_R$ the contact line in this zone begins to recede and the oil-wet area decreases (Fig. 6.11d). Further, two scenarios are possible:

(A) Progressive shrinkage of the oil-wet area until *full detachment* of the oil drop; this has been observed by Mahé et al. [64].
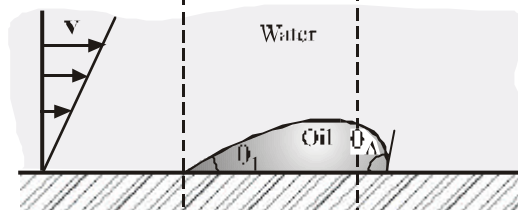
(B) During the shrinkage of the oil-wet area the contact line $q_1$ could become again greater than $q_R$, and the *shrinking of the oil-wet area ceases*. Further, oil-drop detachment is possible at higher shear rate by means of the *emulsification* mechanism, i.e. with the appearance of a

**ROLLING-UP MECHANISM**
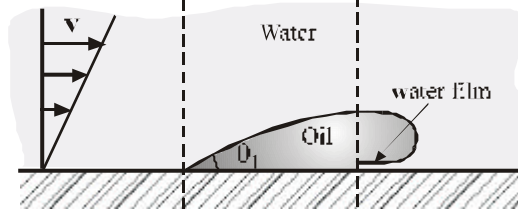**(Destabilization of a Three-Phase Contact Line)**
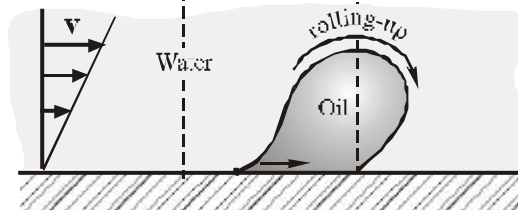
a) The oil-water interface is stable



b) $\theta_2 > \theta_A \Rightarrow$ Spreading without detachment



c) $\theta_A \longrightarrow 180° \Rightarrow$ Formation of water film without detachment



d) For $\theta_1 < \theta_R \Rightarrow$ Detachment of the contact line and rolling-up of the drop



KEY: $\theta_1 < \theta_R$ is a sufficient
condition for rolling-up

Fig. 6.11. (a) For $q_1 > q_R$ and $q_2 < q_A$ the flow cannot cause motion of the contact line. (b) For $q_2 > q_A$ the contact line advances at the leeward side and the oil-wet area increases. (c) For $q_A \rightarrow 180°$ the deformation of the drop leads to the formation of a water film at the leeward side. (d) For $q_1 < q_R$ the contact line at the leeward side recedes and the oil-wet area decreases.

residual drop, see the photographs in Fig. 6.12. In other words, this is a *mixed mechanism* of drop detachment.

*Discussion*. Coming back to the mechanisms for destabilization of an attached oil drop, we can summarize their features in the following way:

(i) *Emulsification* mechanism: Unstable shape (necking) of the oil drop in the shear flow, see Fig. 6.8 and 6.12.

(ii) *Rolling up* mechanism with an *"integral"* criterion for the onset of drop detachment, Eq. (6.41): The total hydrodynamic drag force exerted on the oil drop becomes greater than the retentive capillary force [64]. In other words, this is a violation of the *integral* balance of forces acting on the drop.

(iii) *Rolling up* mechanism with a local criterion for the onset of drop detachment: The contact angle at the stream-ward side becomes smaller than the threshold receding angle,

$$q_1 \leq q_R \qquad \text{(local criterion for drop detachment)} \qquad (6.43)$$

Thus the contact line begins to recede, the oil-wet area decreases, and eventually the drop detaches (Fig. 6.11d). In other words, this is a violation of the *local* balance of forces acting per unit length on the contact line at the stream-ward side.

Intuitively, one may expect that in some cases the criterion (iii) could be satisfied for lower shear rates, as compared to criterion (ii). It is necessary to verify, both theoretically and experimentally, which is the real mechanism of drop detachment, (i), (ii), (iii) or a combination of them. It may happen that for different systems different mechanisms are operative.

As an illustration, in Fig. 6.12 we present consecutive video-frames of the detachment of an oil drop in shear flow; photos taken by Marinov [75]. The water phase is a 0.5 mM solution of sodium dodecyl sulfate (SDS) + 50 mM NaCl. The oil drop is from triolein, a triglyceride which is completely insoluble in the surfactant solution. The oil−water interfacial tension is $s = 20$ mN/m. The substrate is a glass plate, representing the bottom of the experimental channel. The latter has height $H_c = 5$ mm and width $W_c = 6$ mm; the height of the oil drop is $H_d \approx 1.7$ mm. For this geometry the Reynolds number can be estimated as follows

$Q = 0$ cm$^3$/s

$Q = 0.88$ cm$^3$/s

$Q = 1.61$ cm$^3$/s

$Q = 1.64$ cm$^3$/s

$Q_{cr} = 1.76$ cm$^3$/s (detachment- frame # 1)

(detachment- frame # 2)

(detachment- frame # 3)
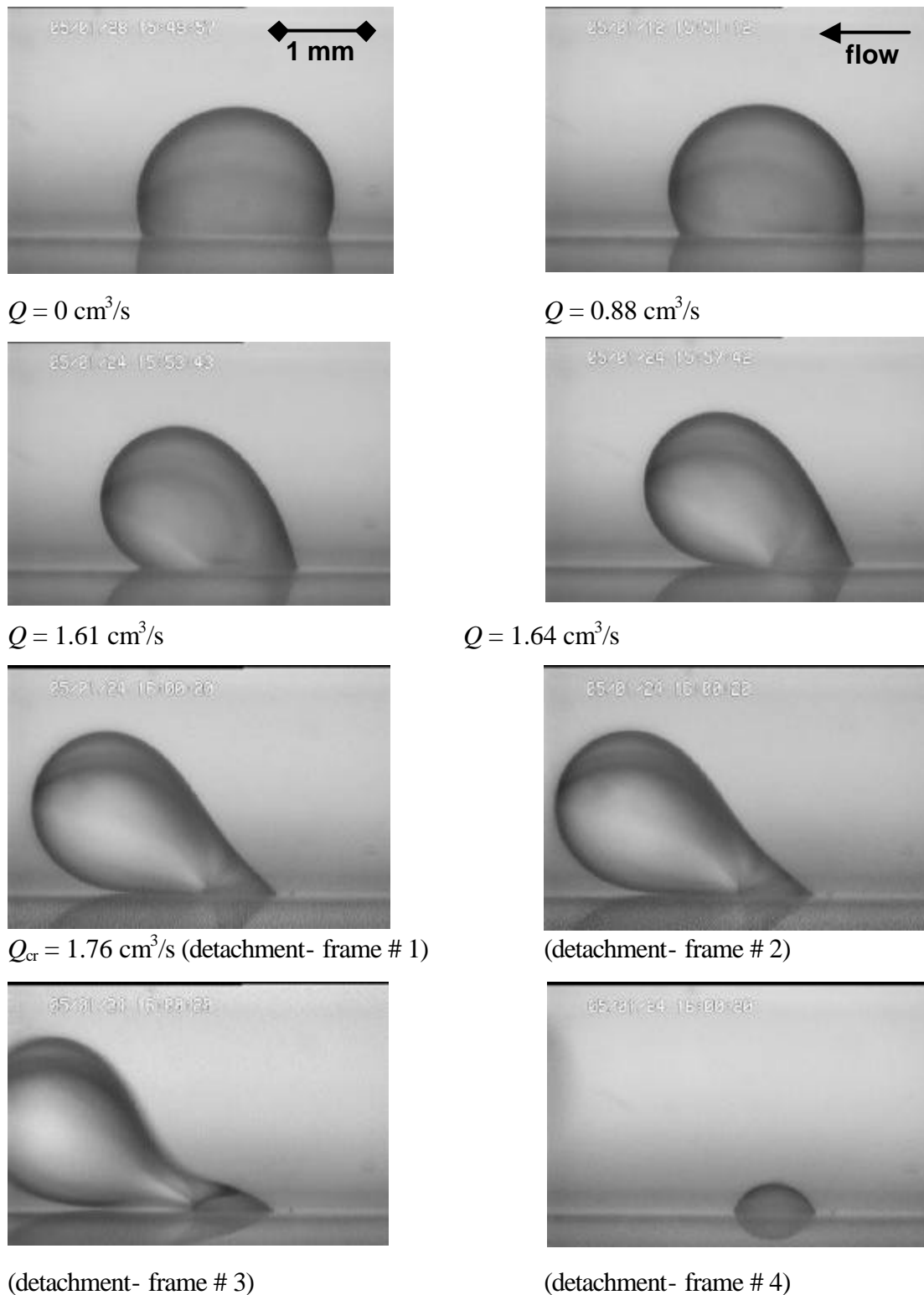
(detachment- frame # 4)

Fig. 6.12. Consecutive stages of detachment of a triolein drop exposed to shear flow. The water phase is a solution of 0.5 mM SDS with 50 mM NaCl at 25°C; $s \approx 20$ mN/m. Each photo corresponds to a given rate of water delivery $Q$. The first four frames show steady state configurations, whereas the last four frames, taken at the same $Q = Q_{cr}$, show stages of the drop detachment (Re$_{cr}$ = 112) [75].

$$\text{Re} = \frac{r_\text{w} Q H_\text{d}}{h_\text{w} W_\text{c} H_\text{c}} \tag{6.44}$$

where $r_\text{w}$ and $h_\text{w}$ are the mass density and the dynamic viscosity of water; $Q$ (cm³/s) is the rate of water delivery in the channel.

In the absence of hydrodynamic flow ($Q = 0$) the oil–water interface is spherical. The video-frames in Fig. 6.12 show the variation of the drop shape with the increase of $Q$. The photos taken at $Q = 1.61$ and 1.64 cm³/s show that the contact line on the stream-ward side has moved and the area wet by oil has shrunk; however, the drop configuration is still stationary (no detachment occurs). The detachment happens at a critical value $Q_\text{cr} = 1.76$ cm³/s; at this rate of water delivery the oil–water interface becomes unstable, necking is observed and eventually a residual drop remains on the substrate; see the last four photos in Fig. 6.12, all of them taken at $Q = Q_\text{cr}$. Hence, in this experimental system the final stage of drop detachment follows the *emulsification* mechanism. The critical value of the Reynolds number, estimated by means of Eq. (6.44) for $h_\text{w}/r_\text{w} = 0.89 \times 10^{-2}$ cm²/s at temperature 25°C is $\text{Re}_\text{cr} \approx 112$.

### 6.3.2. *DETACHMENT OF OIL DROPS PROTRUDING FROM PORES*

If an oil drop is located at the orifice of a pore, there is a strong hysteresis of the contact angle. The experimental video-frames shown in Figs. 6.13 and 6.14 show two mechanisms of detachment of oil drops exposed to *shear flow*. Note that during these experiments the volume of the oil drops has been fixed (no supply of additional oil through the orifice).

*Hydrophobic orifice of the pore.* To mimic such pore we used a glass capillary with hydrophobic inner wall and inner diameter 0.6 mm, Fig. 6.13. The aqueous and oil phases, and the temperature are the same as in Fig. 6.12. When carrying out the experiments special measures have been taken to prevent an entry of the surfactant solution in the capillary, which would cause hydrophilization of its inner wall. The first three photos in Fig. 6.13 show stationary configurations of the drop corresponding to increasing values of the rate of water supply $Q$. The last three frames, taken at the same $Q = Q_\text{cr}$, represent consecutive stages of the drop detachment, which again follows the *emulsification mechanism*. The height and width of the channel are $H_\text{c} = 3$ mm and $W_\text{c} = 5$ mm; the height of the oil drop is $H_\text{d} \approx 1.3$ mm. From Eq. (6.44) with $Q_\text{cr} = 1.39$ cm³/s we estimate $\text{Re}_\text{cr} \approx 135$.

$Q = 0$ cm$^3$/s

$Q = 0.59$ cm$^3$/s

$Q = 1.17$ cm$^3$/s

$Q_{cr} = 1.39$ cm$^3$/s (detachment- frame # 1)

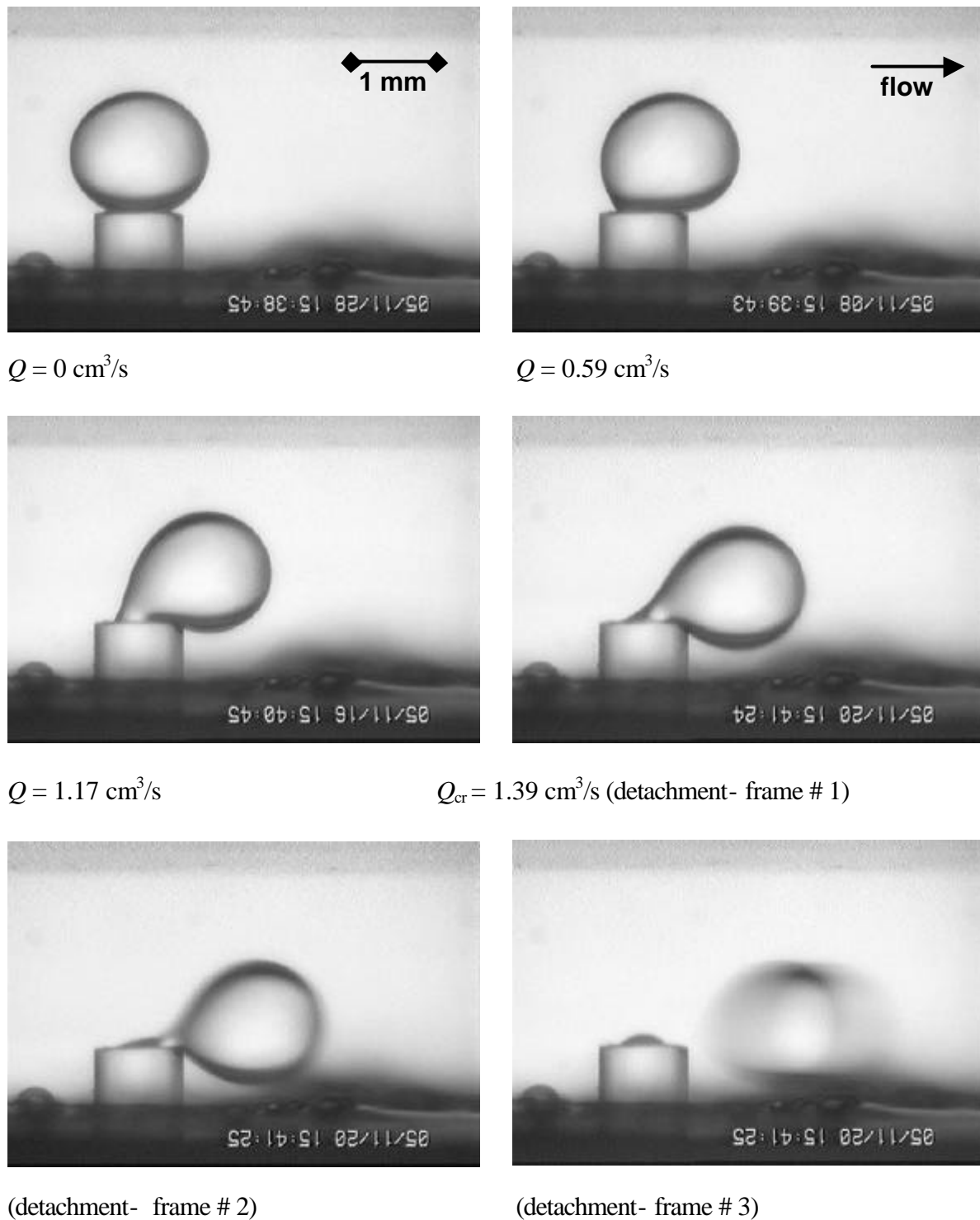(detachment-  frame # 2)

(detachment- frame # 3)

Fig. 6.13. Oil drop at the tip of a glass capillary with *hydrophobized* orifice of inner diameter 0.6 mm: consecutive stages of drop detachment due to applied shear flow. The drop has a fixed volume. The aqueous and oil phases are as in Fig. 6.12. The first three frames show stationary configurations at three fixed rates of water delivery, *Q*. The last three frames, taken at the same $Q = Q_{cr}$, show stages of the drop detachment (Re$_{cr}$ = 135) [75].

$Q = 0$ cm$^3$/s

$Q = 0.88$ cm$^3$/s

$Q_{cr} = 1.05$ cm$^3$/s (detachment - frame # 1)

(detachment - frame # 2)
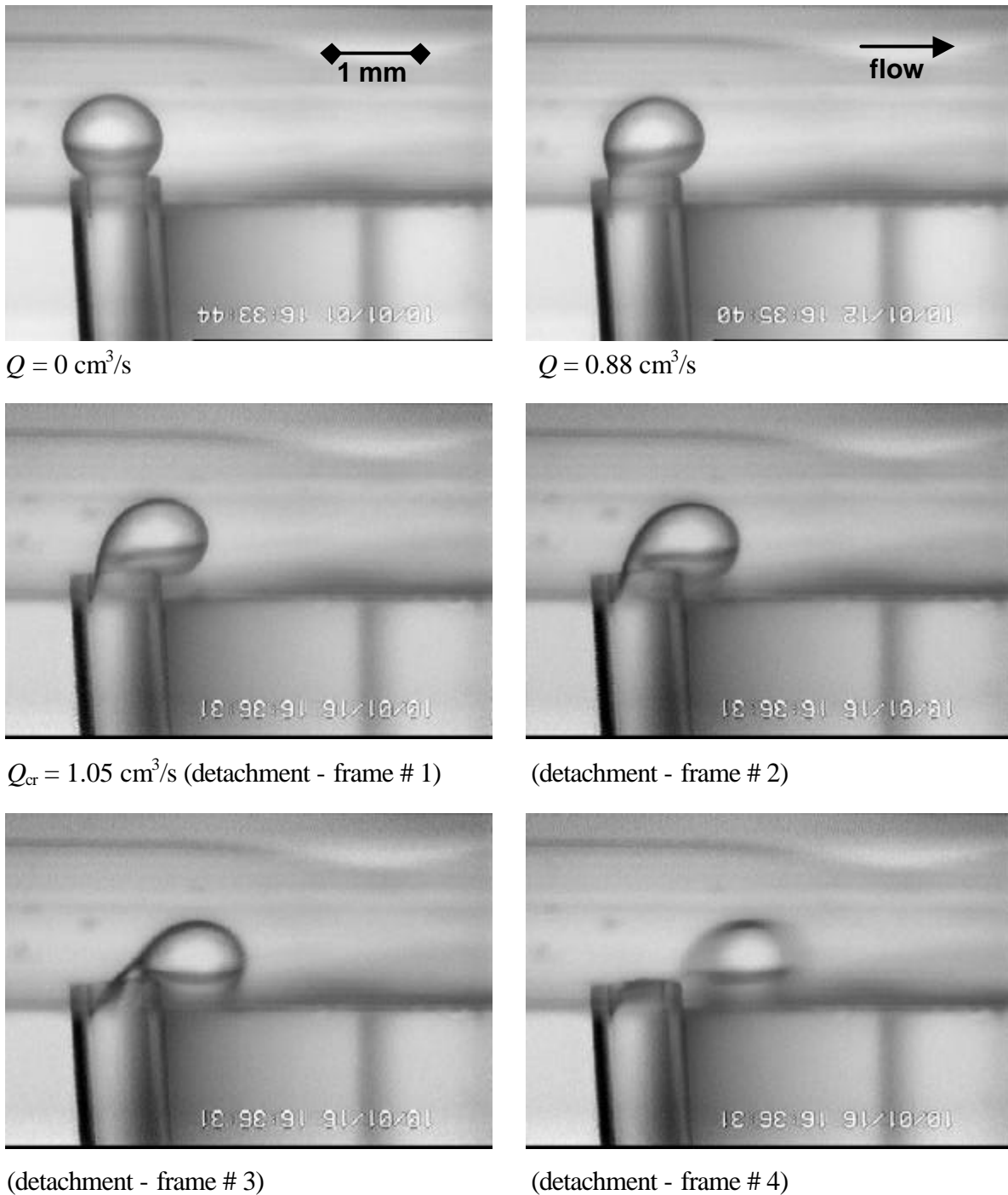
(detachment - frame # 3)

(detachment - frame # 4)

Fig. 6.14. Oil drop at the tip of a glass capillary with *hydrophilized* orifice of inner diameter 0.6 mm: consecutive stages of drop detachment due to applied shear flow. The oily and aqueous phases are the same as in Figs. 6.12 and 6.13, with the only difference that the concentration of SDS is 20 times higher; the interfacial tension is $s = 5$ mN/m. The first two frames show stationary configurations at two fixed rates of water delivery, $Q$. The last four frames, taken at the same $Q = Q_{cr}$, show stages of the drop detachment (Re$_{cr} = 42$) [75].

*Hydrophilic orifice of the pore.* Figure 6.14 shows consecutive video-frames of the detachment of an oil drop protruding from a capillary with hydrophilized orifice. To achieve hydrophobization, first aqueous surfactant solution was let to fill the upper part of the capillary, where its inner wall was hydrophilized owing to the adsorption of surfactant. Next, some amount of oil was supplied to form a protruding oil drop; simultaneously, a water film, sandwiched between oil and glass, was formed in the hydrophilized zone. This water film essentially facilitates the detachment of the oil drop by the shear flow, see Figs. 6.14 and 6.15. The protruding drop is not attached to the solid edge. At higher shear rates, the drop, deformed by the flow, is cut at the edge of the capillary; we could call this the *"edge-cut" mechanism*.

In Fig. 6.14 the height and width of the channel are $H_c = 2$ mm and $W_c = 12.5$ mm; the height of the oil drop is $H_d \approx 0.9$ mm. From Eq. (6.44) with $Q_{cr} = 1.05$ cm$^3$/s we estimate $\text{Re}_{cr} \approx 42$ (compare the latter value with $\text{Re}_{cr} \approx 135$ for the hydrophobic capillary). We may conclude that the hydrophilization essentially facilitates the detachment of an oil drop protruding from an orifice.
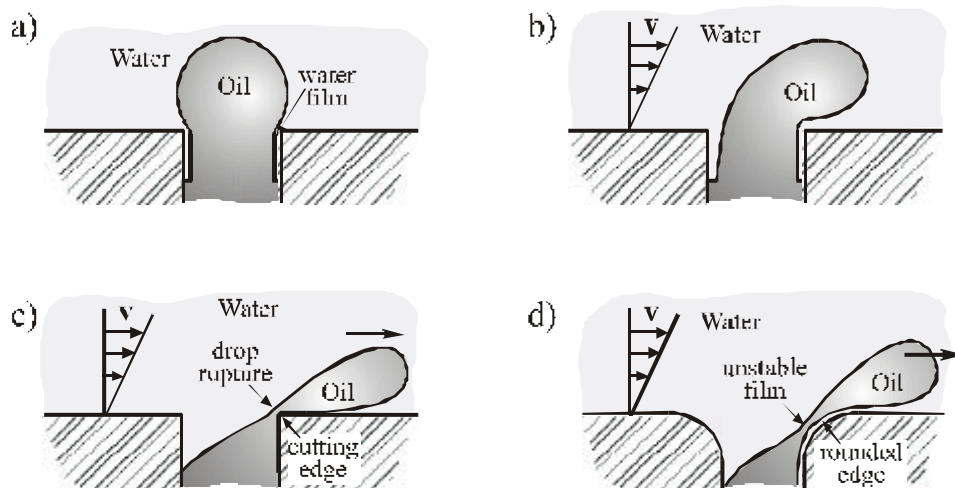
## EDGE-CUT MECHANISM



Fig. 6.15 Scheme of the edge-cut mechanism. (a) In the zone, where the inner wall of the pore is hydrophilized by the surfactant solution, a thin aqueous film separates the oil and solid. (b) In shear flow the oil drop deforms easier because it is not attached to the solid edge. (c) The latter cuts the drop on two parts at a higher shear rate. (d) Even a rounded solid edge could cause splitting of the drop in shear flow because of the instability of the formed oily film.

The situation becomes more complicated when oil is continuously supplied through the capillary (pore) and oil drops are blown out one after another. The experiments show that the radius of the formed drops is from 3.0 to 3.5 times larger than the radius of the capillary, if there is no coalescence of the drops after their formation [55-57]. The latter fact has not yet been explained theoretically. Moreover, it has been observed [76] that if a shear flow is applied, the size of the drops essentially decreases with the rise of the shear rate for Re > 100.

### 6.3.3. *PHYSICOCHEMICAL FACTORS INFLUENCING THE DETACHMENT OF OIL DROPS*

Up to here we considered mostly the role of *mechanical* factors: drag force due to shear flow and retention force related to surface tension and stress balance at the contact line. These factors presume an input of mechanical energy in the system. However, even for a great energy input some residual oil drops could remain on the substrate, see Figs. 6.8c and 6.12, i.e. complete removal of the oil may not be achieved.

An alternative way to accomplish detachment of oil drops is to utilize the action of purely *physicochemical* factors. One of them is related to the *mechanism of the disjoining film*, which is described briefly below.

Historically, such a mechanism has been first observed for polycrystalline solids immersed in liquid, see Fig. 6.16a. If the tension of the solid-liquid interface, $s_{sl}$, is small enough to satisfy the relationship $2s_{sl} < s_g$, where $s_g$ is the surface tension at the boundary between two crystalline grains, then a liquid film penetrates between the grains and splits the polycrystal to small monocrystals. This phenomenon is observed with Zn in liquid Ga, Cu in liquid Bi, NaCl in water [77].

An analogous phenomenon (penetration of disjoining water film) has been observed by Powney [78], Stevenson [79, 80] and Kao et al. [81] for a drop of oil attached to a solid substrate. It is termed also the "diffusional" mechanism. The condition for penetration of disjoining water film between oil and solid is

$$s_{OW} + s_{SW} < s_{SO} \tag{6.45}$$

see Fig. 6.16b for the notation. Equation (6.45) means that a Neumann-Young triangle does not

## DISJOINING-FILM MECHANISM

### a) In Polycrystallites



### b) Attached Drops



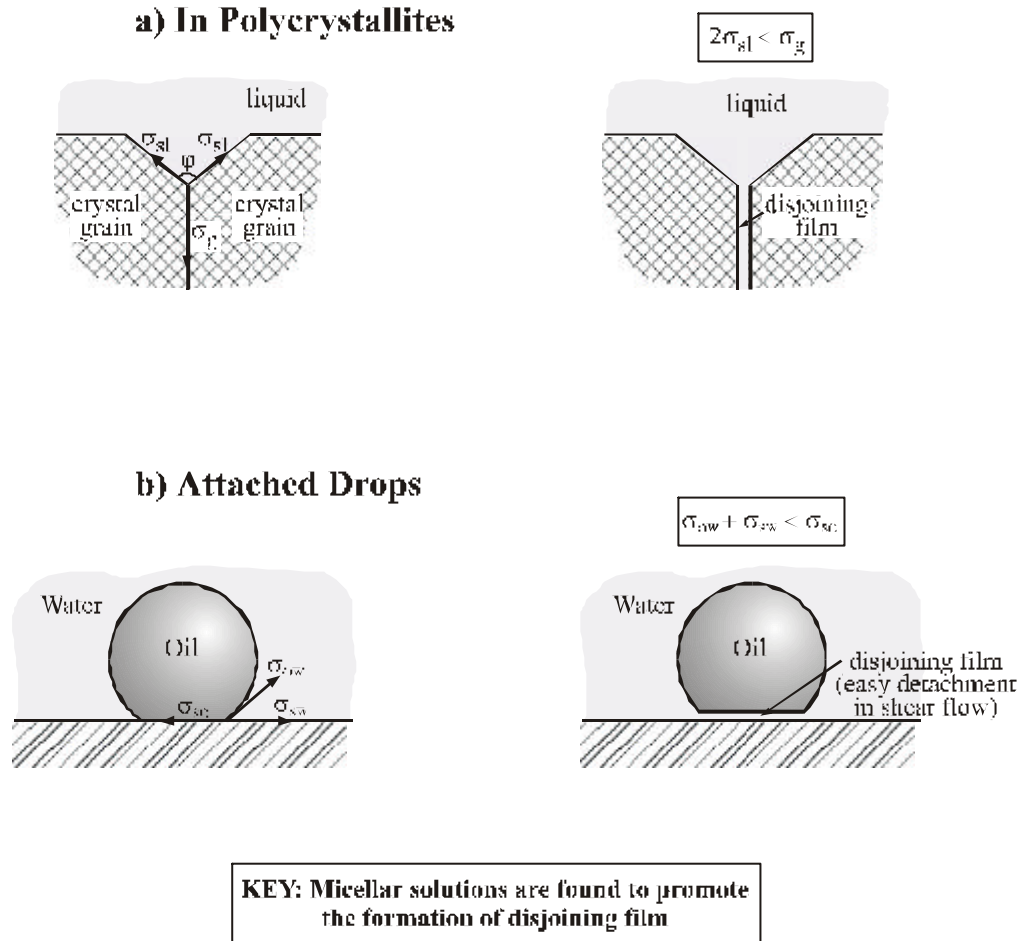**KEY: Micellar solutions are found to promote the formation of disjoining film**

Fig. 6.16. Scheme of the disjoining film mechanism with (a) polycrystallites and (b) oil drop attached to a substrate.

exist, see Chapter 2. For that reason the solid-oil interface is exchanged with a water film, whose surfaces have tensions $s_{OW}$ and $s_{SW}$. Equation (6.45) shows that the formation of such film is energetically favorable. This can happen if a "strong" surfactant, dissolved in the aqueous phase, sufficiently lowers the oil-water and solid-water surface tensions.

In the experiments of Kao et al. [81] drops of crude oil have been detached from glass in solutions of 1 wt% $C_{16}$-alpha-olefin-sulfonate + 1 wt% NaCl. These authors have observed directly the dynamics of water-film penetration. Once the disjoining film has been formed, even a weak shear flow is enough to detach the oil drop from the substrate. The study in Ref. [81] was related to the enhanced oil recovery; however, similar mechanism can be very important also for oil-drop detachment in other

applications of detergency. It is worthwhile noting that not every surfactant could cause penetration of disjoining water film. For each specific system one should clarify which surfactants and surfactant blends give rise to penetration of disjoining films between oil and solid, and how sensitive is their action to the type of oil and substrate.

The major advantage of the disjoining-film mechanism is that it strongly reduces the input of mechanical energy in washing, and effectuates complete washing, i.e. no residual oil drops remain on the substrate. A drawback of this mechanism is that the "strong" surfactant could produce undesirable changes in the properties of the substrate (change of the color of fabrics, irritation action on skin, etc.).

## 6.4.    SUMMARY

In this chapter we consider some aspects of the interaction of colloidal particles with an interface, which involve deformations of a fluid phase boundary and/or hydrodynamic flows. First, from a thermodynamic viewpoint, we discuss the energy changes accompanying the deformation of a fluid particle (emulsion drop of gas bubble) upon its collision with an interface or another particle. Formally, the interaction energy depends on two parameters: the surface-to-surface distance $h$ and the radius $r_c$ of the film formed in the collision zone: $U = U(h,r_c)$, see Eq. (6.1). If the interaction is governed by the surface dilatation and the DLVO forces (van der Waals attraction and electrostatic repulsion), the energy may exhibit a minimum, which corresponds to the formation of a floc of two attached fluid particles with a liquid film between them, see Fig. 6.1a. The depth of this minimum increases if the electrostatic repulsion is suppressed by addition of electrolyte, or if the size of the fluid particle is greater, Fig. 6.1b. When oscillatory-structural forces are operative, then the surface $U(h,r_c)$ exhibits a series of minima separated by energy barriers, Fig. 6.2. When the height of such barrier is greater than $kT$, it can prevent the Brownian flocculation of the fluid particles and may decelerate the creaming in emulsions, Fig. 6.3.

The radius of the liquid film formed between a fluid particle and an interface can be determined by means of force balance considerations. The theory predicts that for small contact angles the film radius must be proportional to the squared radius of the particle, Eq. (6.15). The latter equation agrees excellently with experimental data (Fig. 6.5).

Next we consider the hydrodynamic interactions of a colloidal particle with an interface (or another particle), which are due to hydrodynamic flows in the viscous liquid medium. Each particle is

subjected to the action of a driving force $F$, which is a sum of an external force (gravitational, Brownian, etc.) and the surface force operative in the zone of contact (the thin liquid film), see Eq. (6.21). The theory relates the driving force with the velocity of mutual approach of the two surfaces. The respective relationships depend on the shape of the particle, its deformability and surface mobility. For example, if the particle is spherical and its surface is tangentially immobile, then the velocity is given by the Taylor formula, Eq. (6.20). If the particle is a drop or bubble, it deforms in the collision zone when the width of the gap becomes equal to a certain distance $h_{inv}$ called the "inversion thickness", see Eq. (6.23). After a liquid film of uniform thickness is formed, then the velocity of particle approach is determined by the Reynolds formula, Eq. (6.25). The transition from Taylor to Reynolds regime is also considered, see Eq. (6.28) and Fig. 6.6.

If the surface of an emulsion drop is tangentially mobile (no adsorbed surfactant), then the streamlining by the outer liquid gives rise to a circulation of the inner liquid, which makes the relation between velocity and force dependent on the viscosities of the two liquid phases, see Eq. (6.31). The most complicated is the case when the mobility of the particle surface is affected by the presence of adsorbed soluble surfactant. In this case the connection between velocity and force is given by Eq. (6.33), which takes into account the effects of the Gibbs elasticity, and of the surface and bulk diffusivity of the surfactant molecules. The gradual mutual approach of two fluid particles may terminate when the thickness of the gap between them reaches a certain critical value, at which fluctuation capillary waves spontaneously grow and cause rupturing of the liquid film and coalescence of the fluid particles, see Section 6.2.7.

Finally, we consider the factors and mechanisms for detachment of an oil drop from a solid surface – this is a crucial step in the process of washing. In the presence of shear flow in the adjacent aqueous phase, the oil drop deforms, the oil–water interface acquires a unstable configuration and eventually the drop splits on two parts; this is known as the *emulsification mechanism* of drop removal, see Figs. 6.8 and 6.12. Alternatively, the deformation might be accompanied with destabilization of the contact line (violation of the Young equation), which would lead to detachment of the drop from the substrate: *rolling-up mechanism*, see Fig. 6.11. Special attention is paid to the detachment of oil drops from the orifice of a pore, which essentially depends on whether the inner surface of the pore is hydrophobic or hydrophilic, see Figs. 6.13 − 6.15. The adsorption of some surfactants is able to modify the interfacial tensions in such a way, that an aqueous (disjoining) film can penetrate between the oil drop and the solid surface thus causing drop detachment without any input of mechanical

energy: *disjoining-film mechanism*. The latter purely physicochemical mechanism is illustrated in Fig. 6.16.

## 6.5.  REFERENCES

1.   N.D. Denkov, D.N. Petsev, K.D. Danov, J. Colloid Interface Sci. 176 (1995) 189.

2.   N.D. Denkov, D.N. Petsev, K.D. Danov, Phys. Rev. Lett. 71 (1993) 3226.

3.   K.D. Danov, D.N. Petsev, N.D. Denkov, R. Borwankar, J. Chem. Phys. 99 (1993) 7179.

4.   P.A. Kralchevsky, N.D. Denkov, K.D. Danov, D.N. Petsev, "Effect of Droplet Deform-ability and Surface Forces on Flocculation", In: Proceedings of the 2nd World Congress on Emulsion (Paper 2-2-150), Bordeaux, 1997.

5.   I.B. Ivanov, K.D. Danov, P.A. Kralchevsky, Colloids Surf. A, 152 (1999) 161.

6.   K.G. Marinova, T.D. Gurkov, G.B. Bantchev, P.A. Kralchevsky, "Role of the Oscillatory Structural Forces for the Stability of Emulsions", in: Proceedings of the 2nd World Congress on Emulsions (Paper 2-3-151), Bordeaux, 1997.

7.   K.G. Marinova, T.D. Gurkov, T.D. Dimitrova, R.G. Alargova, D. Smith, Langmuir 14 (1998) 2011.

8.   K.D. Danov, I.B. Ivanov, T.D. Gurkov, R.P. Borwankar, J. Colloid Interface Sci. 167 (1994) 8.

9.   I.B. Ivanov, D.S. Dimitrov, Thin Film Drainage, in: "Thin Liquid Films", I.B. Ivanov (Ed.), Marcel Dekker, New York, 1988; p. 379.

10.   B.V. Derjaguin, M.M. Kussakov, Acta Physicochim. USSR, 10 (1939) 153.

11.   R.S. Allan, G.E. Charles, S.G. Mason, J. Colloid Sci. 16 (1961) 150.

12.   S. Hartland, R.W. Hartley, "Axisymmetric Fluid-Liquid Interfaces", Elsevier, Amsterdam, 1976.

13.   P.A. Kralchevsky, I.B. Ivanov, A.D. Nikolov, J. Colloid Interface Sci. 112 (1986) 108.

14.   E.S. Basheva, Faculty of Chemistry, University of Sofia, private communication.

15.   S.A.K. Jeelani, S. Hartland, J. Colloid Interface Sci. 164 (1994) 296.

16.   I.B. Ivanov, D.S. Dimitrov, P. Somasundaran, R.K. Jain, Chem. Eng. Sci. 40 (1985) 137.

17.   V.G. Levich, "Physicochemical Hydrodynamics", Prentice-Hall, Englewood Cliffs, New Jersey, 1962.

18.   I.B. Ivanov, Pure Appl. Chem. 52 (1980) 1241.

19.   D.A. Edwards, H. Brenner, D.T. Wasan, "Interfacial Transport Processes and Rheology", Butterworth-Heinemann, Boston, 1991.

20.   I.B. Ivanov, P.A. Kralchevsky, Colloids Surf. A, 128 (1997) 155.

21.   D. Möbius, R. Miller (Eds.) "Drops and Bubbles in Interfacial Research", Elsevier, Amsterdam, 1998.

22. K.D. Danov, P.A. Kralchevsky, I.B. Ivanov, in: Encyclopedic Handbook of Emulsion Technology, J. Sjöblom (Ed.), Marcel Dekker, New York, 2001.

23. L.D. Landau, E.M. Lifshitz, "Fluid Mechanics", Pergamon Press, Oxford, 1984.

24. G.I. Taylor, private communication acknowledged by W. Hardy and I. Bircumshaw, Proc. Roy. Soc. London A 108 (1925) 1-18.

25. I.B. Ivanov, B.P. Radoev, T. Traykov, D. Dimitrov, E. Manev, Chr. Vassilieff, in: "Proceedings of the International Conference on Colloid and Surface Science", E. Wolfram (Ed.), Vol.1, p.583, Akademia Kiado, Budapest, 1975.

26. P.A. Kralchevsky, K.D. Danov, I.B. Ivanov, Thin Liquid Film Physics, in: "Foams: Theory, Measurements and Applications", R.K. Prud'homme (Ed.), M. Dekker, New York, 1995, p.86.

27. K.D. Danov, I.B. Ivanov, Critical Film Thickness and Coalescence in Emulsions, in: Proceedings of the 2nd World Congress on Emulsion (Paper No. 2-3-154), Bordeaux, 1997.

28. O. Reynolds, Phil. Trans. Roy. Soc. (London) A177 (1886) 157.

29. M.J. Stefan, Sitzungsberichte der Mathematish-naturwissenschaften Klasse der Kaiserlichen Akademie der Wissenschaften, II. Abteilung (Wien), Vol. 69 (1874) 713.

30. K.D. Danov, N.D. Denkov, D.N. Petsev, R. Borwankar, Langmuir 9 (1993) 1731.

31. E.S. Basheva, T.D. Gurkov, I.B. Ivanov, G.B. Bantchev, B. Campbell, R.P. Borwankar, Langmuir 15 (1999) 6764.

32. E. Rushton, G.A. Davies, Appl. Sci. Res. 28 (1973) 37.

33. S. Haber, G. Hetsroni, A. Solan, Int. J. Multiphase Flow 1 (1973) 57.

34. L.D. Reed, F.A. Morrison, Int. J. Multiphase Flow 1 (1973) 573.

35. G. Hetsroni, S. Haber, Int. J. Multiphase Flow 4 (1978) 1.

36. F.A. Morrison, L.D. Reed, Int. J. Multiphase Flow 4 (1978) 433.

37. V.N. Beshkov, B.P. Radoev, I.B. Ivanov, Int. J. Multiphase Flow 4 (1978) 563.

38. D.J. Jeffrey, Y. Onishi, J. Fluid Mech. 139 (1984) 261.

39. Y.O. Fuentes, S. Kim, D.J. Jeffrey, Phys. Fluids 31 (1988) 2445.

40. R.H. Davis, J.A. Schonberg, J.M. Rallison, Phys. Fluids A1 (1989) 77.

41. X. Zhang, R.H. Davis, J. Fluid Mech. 230 (1991) 479.

42. T.T. Traykov, I.B. Ivanov, International J. Multiphase Flow, 3 (1977) 471.

43. T.T. Traykov, E.D. Manev, I.B. Ivanov, International J. Multiphase Flow, 3 (1977) 485.

44. P.M. Krugljakov, Hydrophile-Lipophile Balance, in: "Studies in Interface Science", Vol. 9, D. Möbius and R. Miller (Eds.), Elsevier, Amsterdam, 2000.

45. A.J. Vries, Rec. Trav. Chim. Pays-Bas 77 (1958) 44.

46. A. Scheludko, Proc. K. Akad. Wetensch. B, 65 (1962) 87.

47. A. Vrij, Disc. Faraday Soc. 42 (1966) 23.

48. I.B. Ivanov, B. Radoev, E. Manev, A. Scheludko, Trans. Faraday Soc. 66 (1970) 1262.

49. I.B. Ivanov, D.S. Dimitrov, Colloid Polymer Sci. 252 (1974) 982.

50. E.D. Manev, S.V. Sazdanova, D.T. Wasan, J. Colloid Interface Sci. 97 (1984) 591.

51. A.K. Malhotra, D.T. Wasan, Chem. Eng. Commun. 48 (1986) 35.

52. N. Munyan, World Oil 8 (1981) 42.

53. M. V. Ostrovsky, E. Nestaas, Colloids Surf. 26 (1987) 351.

54. L. Thompson, J. Colloid Interface Sci. 163 (1994) 61.

55. K. Kandori, Application of Microporous Glass Membranes: Membrane Emulsification, in: "Food Processing: Recent Developments", A. Gaonkar (Ed.), Elsevier, Amsterdam, 1995.

56. V. Schröder, H. Schubert, "Production of Emulsions with Ceramic Membranes", Proc. 2nd World Congress on Emulsion, Vol. 1, Paper No. 1-2-290, Bordeaux, 1997.

57. V. Schröder, O. Behrend, H. Schubert, J. Colloid Interface Sci. 202 (1998) 334.

58. E.A. Evans, Biophys. J. 13 (1973) 941.

59. E.A. Evans, R.M. Hochmuth, J. Membr. Biol. 30 (1977) 351.

60. M.A. Hubbe, Colloids Surf. 12 (1984) 151.

61. M.M. Sharma, H. Chamoun, D.S.H. Sita Rama Sarma, R.S. Schechter, J. Colloid Interface Sci. 149 (1992) 121.

62. K.W. Dillan, E.D. Goddard, D.A. McKenzie, J. Am. Oil. Chem. Soc. 56 (1979) 59.

63. M.C. Gum, E.D. Goddard, J. Am. Oil. Chem. Soc. 59 (1982) 142.

64. M. Mahé, M. Vignes-Adler, A. Rosseau, C.G. Jacquin, P.M. Adler, J. Colloid Interface Sci. 126 (1988) 314.

65. M. Mahé, M. Vignes-Adler, P. M. Adler, J. Colloid Interface Sci. 126 (1988) 329.

66. M. Mahé, M. Vignes-Adler, P. M. Adler, J. Colloid Interface Sci. 126 (1988) 337.

67. A.J. Goldmann, R.G. Cox, H. Brenner, Chem. Eng. Sci. 22 (1967) 653.

68. E.B. Dussan, R.T.-P. Chow, J. Fluid Mech. 137 (1983) 1.

69. S. Basu, K. Nandakumar, J.H. Masliyah, J. Colloid Interface Sci. 190 (1997) 253.

70. R. Finn, "Equilibrium Capillary Surfaces", Springer Verlag, Berlin, 1986.

71. R. Finn, M. Shinbrot, J. Math. Anal. Appl. 123 (1987) 1.

72. S. D. Iliev, J. Colloid Interface Sci. 194 (1997) 287.

73. S. D. Iliev, J. Colloid Interface Sci. 213 (1999) 1.

74. N. K. Adam, J. Soc. Dyers Colour. 53 (1937) 121.

75. G.S. Marinov, Faculty of Chemistry, Univ. of Sofia, private communication.

76. C.A. Paraskevas, Chem. Engineering Department., Univ. Patras, private communication.

77. E.D. Shchukin, A.V. Pertsov, E.A. Amelina, "Colloid Chemistry", Moscow University Press, Moscow, 1982.

78. J. Powney, J. Text. Inst. 40 (1949) 519.

79. D.G. Stevenson, J. Text. Inst. 42 (1951) 194.

80. D. G. Stevenson, J. Text. Inst. 44 (1953) 548.

81. R.L. Kao, D.T. Wasan, A.D. Nikolov, D.A. Edwards, Colloids Surf. 34 (1988) 389.